

Nitrite Cycling in the Primary Nitrite Maxima of the Eastern Tropical North Pacific

Nicole M. Travis¹, Colette L. Kelly¹, Margaret R. Mulholland², Karen L. Casciotti¹

¹ Earth System Science, Stanford University, Stanford CA, 94305, USA

² Department of Ocean, Earth and Atmospheric Science, Old Dominion University, Norfolk VA, 23529, USA

Correspondence to: Nicole M. Travis (ntravis@stanford.edu)

Abstract. The primary nitrite maximum (PNM) is a ubiquitous feature of the upper ocean, where nitrite accumulates in a sharp peak at the base of the euphotic zone. This feature is situated where many chemical and hydrographic properties have strong gradients and the activities of several microbial processes overlap. Near the PNM, four major microbial processes are active in nitrite cycling: ammonia oxidation, nitrite oxidation, nitrate reduction and nitrite uptake. The first two processes are mediated by the nitrifying archaeal/bacterial community, while the second two processes are primarily conducted by phytoplankton. The overlapping spatial habitats and substrate requirements for these microbes have made understanding the formation and maintenance of the PNM difficult. In this work, we leverage high resolution nutrient and hydrographic data and direct rate measurements of the four microbial processes to assess the controls on the PNM in the Eastern Tropical North Pacific. The depths of the nitrite maxima showed strong correlations with several water column features (e.g., top of the nitracline, top of the oxycline, depth of the chlorophyll maximum), whereas the maximum concentration of nitrite correlated weakly with only a few water column features (e.g. nitrate concentration at the nitrite maximum). The balance between microbial production and consumption of nitrite was a poor predictor of the concentration of the nitrite maximum, but rate measurements showed that nitrification was a major source of nitrite in the ETNP, while phytoplankton release occasionally accounted for large nitrite contributions near the coast. The temporal mismatch between rate measurements and nitrite standing stocks suggests that studies of the PNM across multiple time scales are necessary.

Short Summary (500 char.) The primary nitrite maximum is a ubiquitous upper ocean feature where nitrite accumulates, but we still do not understand its formation and the co-occurring microbial processes involved. Using correlative methods and rates measurements, we found strong spatial patterns between environmental conditions and depths of the nitrite maxima, but not the maximum concentrations. Nitrification was the dominant source of nitrite, with occasional high nitrite production from phytoplankton near the coast.

1 Introduction

Nitrogen (N) availability often controls ocean primary productivity through its role as a limiting nutrient (Zehr and Ward, 2002). In marine systems, nitrate makes up over 88% of the bioavailable ('fixed') N pool, with dissolved organic N representing the next largest pool of fixed N (Gruber, 2008). However, the vertical distributions of these species render them unavailable to many of the microbes that require them. For example, nitrate is depleted in euphotic surface

36 waters where primary production is confined, but abundant in waters below the euphotic zone. Other inorganic fixed
37 N species, e.g., nitrite and ammonium, are present in smaller quantities, and their production and consumption are
38 tightly coupled in the marine environment. In the upper ocean, the nitracline demarcates a spatial transition where
39 nitrate, nitrite and ammonium may all be available to microbes simultaneously. In particular, the primary nitrite
40 maximum (PNM) is a ubiquitous feature of the upper ocean. In the Pacific Ocean, the median nitrite concentration
41 across PNM features is 237 nM (Olsen et al., 2020; Key et al., 2015), although concentrations as high as 2.8 μ M have
42 been reported (Brandhorst, 1958; Carlucci et al., 1970; Dore and Karl, 1996; Wada and Hattori, 1972). In addition,
43 nitrite can be present throughout the entire surface water column (Lomas and Lipschultz, 2006; Zakem et al., 2018).
44 The accumulation of nitrite at the PNM occurs at a depth horizon where dynamic N cycling occurs, and it can appear
45 and disappear within the span of only 25 meters. The PNM location generally coincides not only with the top of the
46 nitracline, but also with the depth of the oxycline, the depth of the chlorophyll maximum, and just below or coincident
47 with an ammonium maximum near the base of the euphotic zone (Dore and Karl, 1996; Herbland and Voituriez, 1979;
48 Holligan et al., 1984; Kiefer et al., 1976; Zafiriou et al., 1992; Zakem et al., 2018). The consistent strong spatial
49 relationships between nitrite, nitrate, and chlorophyll concentrations hint at a relationship between these environmental
50 parameters and nitrite production, but does not provide a clear mechanism.

51 Because the PNM sits at a depth where many environmental parameters and microbial N transformations are in
52 transition, determining the exact controls on nitrite accumulation in the PNM remains difficult (Lomas and Lipschultz,
53 2006; Wan et al., 2021; Zakem et al., 2018; Wan et al., 2018). Near the PNM, the three main microbial groups involved
54 in nitrite cycling are ammonia oxidizers, nitrite oxidizers and phytoplankton. Nitrification comprises the oxidation of
55 ammonia to nitrate with nitrite as an intermediate. Archaeal ammonia oxidizers dominate the oxidation of ammonia
56 to nitrite (Francis et al., 2007, 2005; Mincer et al., 2007; Santoro et al., 2010; Schleper et al., 2005) while bacterial
57 nitrite oxidizers convert nitrite to nitrate (Lücker et al., 2010, 2013; Watson and Waterbury, 1971; Ward and Carlucci,
58 1985). Many phytoplankton can also both produce and consume nitrite. Traditionally, phytoplankton are thought to
59 be consumers of inorganic N, but it is now well documented that they also release inorganic N, including nitrite (Al-
60 Qutob et al., 2002; Collos, 1998, 1982a; Lomas and Glibert, 2000). Nitrification and photosynthesis can co-occur near
61 the depth of the PNM, so the extent to which they contribute to PNM formation and what factors influence the
62 magnitude and depth of the PNM depends on how these microbes interact and transform nitrogen and how microbial
63 physiologies respond to gradients in environmental conditions (Ward et al., 1989).

64 The combination of each microbial group's physiological responses to environmental parameters controls the vertical
65 profiles of concentrations of different N species and leads to accumulation of nitrite at the PNM. Imbalance between
66 the two steps of nitrification has been used to explain nitrite accumulation; variations in light levels may cause
67 differential photoinhibition or differential recovery from photoinhibition of nitrite oxidizers leading to accumulation
68 of nitrite (Guerrero and Jones, 1996; Olson, 1981). Ammonia-oxidizing bacteria are less sensitive to light, have quicker
69 recovery times to light stress, and are active at higher rates under light stress compared to nitrite-oxidizing bacteria
70 (Guerrero and Jones, 1996; Olson, 1981). Recent studies focusing specifically on the numerically dominant ammonia
71 oxidizing archaea (AOA), have shown high variation in light tolerance across AOA phylotypes which may explain

72 the lack of strong light inhibition of ammonia oxidation in some studies (Horak et al., 2018; Merbt et al., 2012; Smith
73 et al., 2014). Additionally, nitrification rates are substrate-dependent and constrained to places and times when
74 ammonia and nitrite are both available (Martens-Habbena et al., 2009) . Nitrite is also taken up by phytoplankton but
75 this process is thought to be light dependent (Lomas and Glibert, 2000; Mulholland and Lomas, 2008) . Nitrite release
76 from phytoplankton is also well documented in culture studies (Al-Qutob et al., 2002; Collos, 1998), but it is still
77 unclear whether nitrite release occurs during incomplete nitrate reduction under low light conditions when energy for
78 its complete assimilation is limited, under fluctuating high light conditions as a photoprotective mechanism, or as a
79 stress response to high light levels (Collos, 1982b; Kiefer et al., 1976; Lomas and Glibert, 1999, 2000; Wada and
80 Hattori, 1971).

81 Accumulation of nitrite occurs when the rate of its production exceeds that of its loss via consumption or diffusion.
82 Thus, the presence of the PNM is an indicator of conditions where production and consumption of nitrite are, or have
83 recently been, imbalanced (Hattori and Wada, 1971). The accumulation of nitrite in the PNM may provide valuable
84 insight into the balance of relative rates of microbial nitrite cycling in the upper ocean, as it indicates a zone where
85 biologically mediated processes are not in balance and may be experiencing differential inhibition or limitation. Rarely
86 are the four major microbial processes related to PNM formation (ammonia oxidation, nitrite oxidation, nitrate
87 reduction and nitrite uptake) measured simultaneously in the field. The few paired rate measurements that exist tend
88 to show that ammonia oxidation rates exceed nitrite oxidation rates in the PNM, suggesting nitrite oxidation is the rate
89 limiting step in the reaction pair and a potential mechanism for nitrite accumulation (Beman et al., 2013; Schaefer and
90 Hollibaugh, 2017; Füssel et al., 2012; Peng et al., 2015; Santoro et al., 2013; Ward et al., 1982). However, the lack of
91 paired measurements focused on the sharp PNM boundaries limits our understanding of the coupling between the two
92 steps of nitrification or other processes affecting nitrite accumulation across these depths. Higher resolution paired
93 measurements will allow us to investigate how environmental gradients create vertical zonation in the relative rates of
94 nitrite-cycling processes that lead to nitrite accumulation within narrow depth horizons. Previous investigations of the
95 PNM have typically focused on nitrifier communities or phytoplankton communities separately, although it is
96 understood that the niches of these communities overlap, and that both may contribute to nitrite accumulation. The
97 studies that have measured both phytoplankton and nitrifier processes (Mackey et al., 2011; Santoro et al., 2013; Wan
98 et al., 2018; Ward, 2005) support the idea that physiological constraints and competitive interactions between these
99 groups drive resource use and nitrite accumulation (Smith et al., 2014; Wan et al., 2021; Zakem et al., 2018).

100 Understanding the controls on rates of co-occurring nitrite cycling processes will help clarify the distributions of
101 microbial activity and how relative rates of these processes may change due to future environmental perturbations.
102 For example, understanding the controls on and patterns of nitrification in the surface ocean is critical for
103 understanding new production, as estimates suggest more than 30% of oceanic primary production is supported by
104 nitrate supplied by nitrification in the euphotic zone (Santoro et al., 2010; Ward et al., 1989; Yool et al., 2007). In
105 addition, the relative contributions of nitrification and phytoplankton activity to the formation of the PNM may also
106 be important for understanding the potential for nitrous oxide formation in the surface ocean (Burlacot et al., 2020;
107 Kelly et al., 2021; Plouviez et al., 2019; Santoro et al., 2011).

108 To investigate the relative contributions of nitrification and phytoplankton processes to net accumulation of nitrite at
109 the PNM feature, we measured rates of four microbially-mediated nitrite cycling processes (ammonia oxidation, nitrite
110 oxidation, nitrate reduction and nitrite uptake) in vertical profiles through the PNM. We analyzed spatial and regional
111 variations in environmental conditions and water column features associated with the PNM, as well as the rates of
112 nitrite production and consumption.

113 **2 Methods**

114 **2.1 Hydrography and nutrient analyses**

115 This study is based on data collected from four cruises to the Eastern Tropical North Pacific Ocean (ETNP) between
116 April 2016 and June 2018 (RB1603 – *R/V Ronald Brown*, April 2016; SKQ201617s – *R/V Sikuliaq*, December 2016;
117 SR1805 – *R/V Sally Ride*, April 2018; and FK180624 – *R/V Falkor*, June 2018; Figure 1). The ETNP hosts one of the
118 largest oceanic oxygen deficient zones (ODZs) and is a region of active nitrogen cycling. Oxygen concentrations
119 decline precipitously from saturated surface water concentrations to nanomolar levels across the oxycline in much of
120 the study area (Cline and Richards, 1972), with oxygen deficient waters beginning as shallow as 15 m at some coastal
121 stations. This study focused on nitrite cycling in the upper water column near the PNM, and all rate data were collected
122 in oxygenated waters in or above the oxycline.

123 Fifty-three stations were occupied during these cruises, and hydrographic observations of temperature, salinity, and
124 oxygen were made using a CTD package (RB1603 – Sea-Bird SBE 11+ CTD, SKQ201617s/SR1805/FK180624 –
125 Sea-Bird SBE 911+ CTD). Fluorescence and photosynthetically active radiation (PAR) measurements were measured
126 at a subset of stations (RB1603 – LiCor Biospherical Photosynthetically Active Radiation Sensor/SeaPoint
127 Chlorophyll Fluorometer). Discrete water samples were collected from Niskin bottles mounted to the CTD rosette to
128 measure dissolved inorganic N concentrations. Nitrite and ammonium concentration measurements were typically
129 made immediately onboard the ship, while samples for nitrate concentration measurements were 0.22 μm filtered and
130 frozen in 60-ml HDPE bottles for analysis at a shore-based laboratory. During the 2016 cruise, a pump profiling system
131 (PPS; as described in Codispoti et al., 1991) was also deployed with a separate CTD package (Seabird SBE19+,
132 WetStar Fluorometer) at all 16 stations.

133 For all cruises, nitrite concentrations were measured colorimetrically with a detection limit of ~200 nM (Strickland
134 and Parsons, 1972). Briefly, five ml of sample water from each Niskin bottle was reacted with 200 μl each of
135 sulfanilamide and N-(1-NAPHTHYL)ethylenediamine reagents, and absorbance at 543 nm was measured after a 10
136 min reaction time and converted to concentration using a standard curve, with an overall precision of $\pm 0.006 \mu\text{M}$.
137 Ammonium concentrations were measured shipboard using a fluorometric method after derivatization with ortho-
138 phthaldialdehyde (OPA) reagent (Holmes et al., 1999). Samples and standards were reacted with OPA for ~8 hours at
139 4°C in the dark before measurement. Detection limit for this ammonia method was 30 nM. In 2016, samples for nitrate
140 plus nitrite were collected from discrete depths using Niskin bottles mounted to a CTD rosette and analyzed shipboard
141 using an Astoria Pacific autoanalyzer according to the manufacturer’s specifications using standard colorimetric

142 methods (Strickland and Parsons, 1972). In 2017, nitrate plus nitrite samples were analyzed using standard
 143 colorimetric methods on a Technicon Autoanalyzer at the University of Washington. In 2018, nitrate plus nitrite was
 144 measured after Cd reduction using a WestCo SmartChem 200 Discrete Analyzer at Stanford University, with an
 145 overall precision of $\pm 0.6 \mu\text{M}$ and detection limit of 85 nM (Miller and Miller, 1988; Rajaković et al., 2012). Nitrate
 146 concentrations were calculated by subtracting nitrite from the concentration of nitrate plus nitrite for all cruises. During
 147 the 2016 cruise (RB1603), cast water from the PPS was pumped directly through a Fast Repetition Rate Fluorometer
 148 (FRRF) for chlorophyll *a* fluorescence measurements and then to an Alpkem Astoria-Pacific rapid-flow analysis
 149 system for near-continuous profiles of nitrate, nitrite, and ammonium concentrations at one measurement per second
 150 and binned to every meter (Holmes et al., 1999; Sakamoto et al., 1990; Strickland and Parsons, 1972).

151 Water column profiles were analyzed to determine station-specific water column features (Table S1). The depth of the
 152 top of the nitracline (Z_{nit}) was identified as depth at which nitrate concentration increased by $1 \mu\text{M}$ compared to a
 153 reference depth of 20 m (Cornec et al., 2021). In addition, the standard nitracline depth (Z_{mnit}) was identified as where
 154 the nitrate gradient was steepest. Similarly, the top of the oxycline (Z_{oxy}) was identified as the depth at which oxygen
 155 concentration decreased by $5 \mu\text{M}$ relative to the concentration at a depth of 20 m. The standard oxycline depth (Z_{moxy})
 156 was where the oxygen gradient was steepest. Other station-specific water column features included the depth and
 157 concentration of the nitrite maximum (m and μM , respectively), the depth and concentration of the chlorophyll
 158 maximum (m and mg m^{-3} , respectively), the depth and concentration of the ammonium maximum (m and nM,
 159 respectively), and the depth at which 1% of the surface photosynthetically active radiance (PAR) was present (m).
 160 Concentrations/characteristics of these variables at the depth of the nitrite maximum were also calculated (e.g., nitrate
 161 concentration ($\text{NO}_3^-_{\text{pnm}}$), chlorophyll concentration (Chl_{pnm}), ammonium concentration ($\text{NH}_4^+_{\text{pnm}}$), oxygen
 162 concentration ($\text{O}_{2\text{pnm}}$), temperature (T_{pnm}), density (D_{pnm}), percent of surface PAR (PAR_{pnm}). The Brunt-Väisälä
 163 frequency (BV_{pnm}) was calculated at the PNM nitrite maximum (± 8 m) using the equation $N = \sqrt{\frac{-g}{\rho} * \frac{d\rho}{dz}}$, where g is
 164 the acceleration due to gravity (m s^{-2}), z is depth (m) and ρ is density (kg m^{-3}). Depth-integrated concentrations of
 165 nitrate, nitrite, and ammonium ($\mu\text{mol N m}^{-2}$) were calculated for the euphotic zone (upper 120 m), capturing the
 166 entirety of the PNM feature.

167

168 **Table 1. Water Column Feature Acronyms, Definitions and Units**

169 Symbol	Definition	Unit
PNM	Primary nitrite maximum, whole feature	–
Chl_{max}	Concentration of the deep chlorophyll maximum	mg m^{-3}
$\text{NH}_4^+_{\text{max}}$	Concentration of the ammonium maximum	nM
$\text{NO}_2^-_{\text{max}}$	Concentration of the nitrite maximum	μM
Z_{chl}	Depth of the deep chlorophyll maximum	m
Z_{NH_4}	Depth of maximum ammonium	m
Z_{NO_2}	Depth of maximum nitrite	m

170

Z_{nit}	Depth of top of the nitracline	m
Z_{mnit}	Depth of steepest gradient in nitracline	m
Z_{oxy}	Depth of the top of the oxycline	m
Z_{moxy}	Depth of steepest gradient in oxycline	m
Z_{PAR}	Depth of 1% surface PAR	m
Chl_{pnm}	Chlorophyll concentration at the PNM peak	mg m^{-3}
$\text{NH}_4^+_{\text{pnm}}$	Ammonium concentration at the PNM peak	nM
$\text{NO}_3^-_{\text{pnm}}$	Nitrate concentration at the PNM peak	μM
T_{pnm}	Temperature at the PNM peak	C
D_{pnm}	Density at the PNM peak	kg m^{-3}
PAR_{pnm}	Percent of surface PAR at the PNM peak	%
$\text{O}_{2\text{pnm}}$	Oxygen concentration at the PNM peak	μM
BV_{pnm}	Brunt Väisälä Frequency at the PNM peak	s^{-1}
$\text{NH}_4^+_{\text{Int}}$	Depth integrated ammonium over upper 120 m	nmol N m^{-2}
$\text{NO}_2^-_{\text{Int}}$	Depth integrated nitrite over upper 120 m	$\mu\text{mol N m}^{-2}$
$\text{NO}_3^-_{\text{Int}}$	Depth integrated nitrate over upper 120 m	$\mu\text{mol N m}^{-2}$
Chl_{Int}	Depth integrated chlorophyll over upper 120 m	mg m^{-2}

171

172 2.2 Nitrite cycling rates

173 Rates of ammonia oxidation, nitrite oxidation, nitrate reduction and nitrite uptake were measured at 12 of the 53
174 stations occupied over 4 cruises from 2016-2018 (Fig. 1a), including five stations from 2016, two stations in 2017,
175 and five stations in 2018. At each of these stations during a pre-dawn cast, 3-4 depths near the PNM were sampled
176 based on real-time CTD fluorescence data during the downcast, targeting depths both within the chlorophyll maximum
177 and on the upslope and downslope of its peak (Table S1). When available, nitrite profiles from previous casts were
178 consulted to guide sampling based on the location of the PNM within the chlorophyll maximum.

179 From each depth, six clear 500-ml polycarbonate (PC) Nalgene bottles were triple-rinsed and filled directly from the
180 Niskin bottle for light incubations. Additionally, six 500-ml or 1-L amber high-density polyethylene (HDPE) Nalgene
181 bottles were triple-rinsed and filled for paired dark incubations. One of three ^{15}N -labeled nitrogen substrates ($\text{K}^{15}\text{NO}_3^-$
182 enriched at 99.5 atm%, $\text{Na}^{15}\text{NO}_2^-$ enriched at 98.8 atm% or $^{15}\text{NH}_4\text{Cl}$ enriched at 99.5 atm%) was added to duplicate
183 bottles to achieve enrichments of 200 nM ^{15}N . High tracer enrichment in samples with low ambient concentrations
184 may lead to enhancement of rates, which are best characterized as potential rates; care must be taken when interpreting
185 results. After gentle mixing, a 60 ml subsample was syringe-filtered (0.22 μm pore size Sterivex) to determine initial
186 concentration and ^{15}N enrichment of the substrate pool. Approximately 10 ml was used for shipboard measurement of
187 the initial concentrations of total nitrite or ammonium (ambient concentration plus ^{15}N -labeled DIN addition). The
188 remaining 50 ml was frozen at $-20\text{ }^\circ\text{C}$ in a 60-ml HDPE bottle for measurement of total nitrate concentration and
189 isotopic enrichment in a shore-based laboratory.

190 Each incubation bottle was placed in a deck-board incubator that approximated the ambient light level from the sample
191 collection depth, achieved using neutral density screening. The percent PAR in the incubators was recorded using a
192 submersible Licor PAR meter or an *in situ* HOBO light and temperature logger (~1%,~4%,~20% surface PAR).
193 Incubators were plumbed with flow-through surface seawater to maintain a consistent water temperature. However,
194 surface water temperatures were often significantly warmer than those at collection depth and could have biased some
195 of the incubation results. Subsamples were collected from each incubation bottle after approximately 8, 16 and 24 hrs.
196 Samples were syringe-filtered (0.22 µm pore size Sterivex) and frozen in 60-ml HDPE bottles for nutrient and isotope
197 analysis in a shore-based laboratory. At the end of the incubation (24 hr), the remaining ~300 ml of water in each
198 replicate bottles was combined in order to maximize the amount of nitrogen available for isotope analysis. Sample
199 water was filtered onto a pre-combusted (450°C for > 4 h) GF/F (0.7 µm) filter; the filter was folded and placed into
200 a cryovial and stored at -80 °C for later analysis of particulate $\delta^{15}\text{N}$ at the University of Hawaii Isotope Lab. All
201 seawater samples were stored frozen until the time of isotopic analysis. Incubation bottles were acid washed and re-
202 used for experiments using the same ^{15}N substrate.

203 **2.3 Isotope analysis and rate calculations**

204 For estimates of ammonia oxidation, nitrite oxidation and nitrate reduction rates, samples collected from each
205 timepoint were analyzed for ^{15}N enrichment of the respective product pool (Table 2). For each sample, the product
206 was converted to nitrous oxide either by bacterial (*P. aureofaciens*) conversion using the denitrifier method (McIlvin
207 and Casciotti, 2011; Sigman et al., 2001) or chemical conversion using the azide method (McIlvin and Altabet, 2005).
208 Isotopic analysis via the denitrifier method was used for measurement of $^{15}\text{NO}_x$ (ie. $^{15}\text{NO}_3^- + ^{15}\text{NO}_2^-$) in ammonia
209 oxidation and nitrite oxidation experiments. Measurements of nitrite oxidation required pre-treatment of samples to
210 remove any remaining $^{15}\text{N-NO}_2$ prior to analysis of $\delta^{15}\text{N-NO}_3$ (Granger and Sigman, 2009). Briefly, 10 ml of each
211 sample was treated with 100 µl of 4% sulfamic acid in 10% hydrochloric acid for 15 min, after which the pH was
212 neutralized using 85 µl of 2M sodium hydroxide before proceeding with denitrifier method. Samples were prepared
213 in volumes targeting 20 nmoles nitrate. The azide method was used to prepare nitrite produced from nitrate reduction
214 experiments for isotopic analysis (McIlvin and Altabet, 2005). Nitrite was converted to nitrous oxide by incubating
215 for ~30 min with a 2M sodium azide solution in 20% acetic acid. The reaction was neutralized with 6M sodium
216 hydroxide prior to isotope analysis. Since nitrite product concentrations were low (<2 µM), a significant portion of
217 the nitrite in the samples was newly created from ^{15}N -labeled nitrate, thus carrier nitrite (5-10 nmoles) of known
218 isotope value was added to dilute the ^{15}N enrichment and increase overall concentration of nitrite in the samples before
219 isotopic analysis. Samples were analyzed in volumes targeting 10 nmoles of nitrite.

220 The isotopic composition of the nitrous oxide produced from each sample was measured in the Casciotti Laboratory
221 at Stanford University using an isotope ratio mass spectrometer (Thermo-Finnigan Delta^{PLUS} XP) fitted with a custom
222 purge-and-trap gas purification and concentration system (McIlvin and Casciotti, 2011). Each set of 9 samples was
223 bracketed with international reference materials to correct for instrument drift and sample size, and to calibrate isotope
224 values. USGS32, USGS34, and USGS35 (Böhlke et al., 2003) were used to calibrate nitrate isotope analyses, and

225 RSIL-N23, N7373 and N10219 (Casciotti et al., 2007) were used to calibrate nitrite isotope analyses. For nitrate
 226 reduction samples, additional mass balance corrections were made to correct for the addition of nitrite carrier to the
 227 product pool before calculation of rates. The denitrifier method for natural abundance nitrate isotope analyses typically
 228 has a precision of better than 0.5‰ for $\delta^{15}\text{N}$ (McIlvin and Casciotti, 2011; Sigman et al., 2001), although standard
 229 deviations are often higher for isotopically enriched samples. Here, the mean analytical precision of $\delta^{15}\text{N-NO}_x$, $\delta^{15}\text{N-}$
 230 NO_3 , $\delta^{15}\text{N-NO}_2$ measurements of ^{15}N -labeled samples were $\pm 4.2\%$, $\pm 4.6\%$ and $\pm 0.7\%$, respectively, corresponding
 231 to mean coefficient of variance (CV%) of 5.3%, 0.56% and 9.7%, respectively (Table 2).

232 **Table 2. Nitrite cycling reactant and product pools as analyzed by isotope rate mass spectrometry.**

233

Microbial Process	^{15}N -labeled Reactant	Prep Method	^{15}N -labeled Product	Mean Precision (‰)	Mean CV %
<i>Ammonia Oxidation</i>	NH_4Cl	Denitrifier	$\text{NO}_3^-/\text{NO}_2^-$	4.2	5.3
<i>Nitrite Oxidation</i>	NaNO_2	Sulfamic-treated + Denitrifier	NO_3^-	4.6	0.56
<i>Nitrate Reduction</i>	KNO_3	Azide w/carrier	NO_2^-	0.7	9.7

234

235

236 Rate calculations were made by tracking the increase in product ^{15}N over the incubation period (Ward, 1985). For
 237 ammonia oxidation the equation is as follows:

$$238 \quad V_{\text{NH}_3} = \frac{\Delta[^{15}\text{NOX}]_{t_8-t_0}}{af^{15}\text{NH}_3_{t_0} \times \Delta t \times 24} \quad (1)$$

239 where $\Delta[^{15}\text{NOX}]_{t_8-t_0}$ is the change in product $^{15}\text{NO}_x$ concentration between the start of the incubation and the 8 h
 240 timepoint (nM), $af^{15}\text{NH}_3_{t_0}$ is the atom fraction of $^{15}\text{NH}_3$ substrate available at the start of the incubation period,
 241 and Δt is the change in time (hours). While the initial ^{15}N in the substrate pool was directly measured at time zero
 242 for use in rate calculations, the addition of 200 nM ^{15}N tracer led to variable atom fraction of ^{15}N in the substrate
 243 pool across experiments, which was calculated from ambient and tracer substrate concentrations. Paired dark and
 244 light incubation samples were used to convert hourly rates to daily rates using a simple assumption of a 12 hr
 245 light:12 hr dark daily cycle. The ammonia oxidation rate, V_{NH_3} , is thus reported in units of nM N day⁻¹. A similar
 246 equation was used to calculate nitrite oxidation and nitrate reduction rates, substituting the appropriate substrate and
 247 product species for each process (Table 1). Some dark incubation data were not available for nitrate reduction
 248 measurements in 2016, so those daily rates were calculated using 24 hr light incubated rates and may be
 249 overestimates. The 16 h and 24 h time point samples were analyzed but not used to calculate rates as experiments
 250 showed non-linear trends after 8 hours of incubation due to substrate depletion. Based on a threshold increase in
 251 product $\delta^{15}\text{N}$ compared to the initial product, a theoretical detection limit was calculated to estimate the rate we can
 252 reasonably expect to discern from zero (Santoro et al., 2013). This calculation is sensitive to both the $\delta^{15}\text{N}$ of the
 253 substrate pool, the concentration of the product pool, and the CV% for $\delta^{15}\text{N}$ measurements. The threshold for
 254 detectable change in product $\delta^{15}\text{N}$ was approximated using the maximum CV% for each experiment. For example, if
 255 the standard deviation in replicates for a sample with a $\delta^{15}\text{N}$ of 25‰ was ± 0.6 , a CV% of 2.4% was used as the

256 theoretical detectable difference between initial and final ^{15}N enrichment in the product pool. Where available, the
257 maximum CV% for each experimental unit was used to calculate the theoretical limit of detection for each depth
258 (Table S1b). The mean theoretical detection limits for ammonia oxidation, nitrite oxidation and nitrate reduction
259 were 0.5, 6.9, and 0.9 nM day^{-1} , respectively. Experimental bottle duplicates were conducted for most rate
260 measurements and those standard deviations are reported with the final rate data (Table S1b).

261 Filters from nitrite uptake rate experiments were dried overnight and packed in tin capsules before shipment to the
262 Biogeochemical Stable Isotope Facility at the University of Hawaii, where samples were analyzed on a Thermo
263 Scientific Delta V Advantage isotope ratio mass spectrometer coupled to a Costech Instruments elemental analyzer.
264 Rate calculations relied on ^{15}N enrichment of the particulate organic nitrogen over the 24 h incubation period as in
265 Dugdale and Goering (1967). Uptake rates were calculated according to Dugdale and Wilkerson (1986) where the
266 initial ^{15}N atom percent fraction of the reactant pool was calculated assuming 0.3663 for the ^{15}N atom percent of the
267 ambient substrate pool and 98.8 atm% $^{15}\text{N-NO}_2^-$ of the isotope tracer addition. Nitrite uptake rates may be
268 underestimated due to dilution of the substrate pool via regeneration over the 24 incubation period, and loss of tracer
269 to unmeasured DON pools (Bronk et al., 1994; Glibert et al., 2019). No correction was made for possible rate
270 enhancement due to tracer addition (Dugdale and Wilkerson, 1986).

271 **2.4 Multiple Linear Regression Analysis**

272 Multiple linear regression (MLR) models were built to assess the environmental variables that influence the depth and
273 magnitude of the PNM feature in the ETNP. The first set of MLR models ('full' models) used semi-continuous
274 measurements (temperature, density, oxygen, chlorophyll fluorescence, PAR, nitrate, nitrite and ammonium) from
275 CTD/PPS casts collected at 16 stations on the 2016 cruise to predict nitrite concentration. Nitrate, nitrite and
276 ammonium data were natural-log transformed to satisfy normal distribution assumptions of the multiple linear
277 regression analyses. Using the R package *leaps*, the model was optimized using a best-subsets selection of the full
278 variable set to maximize R^2 and minimize root mean squared error for each potential model size using 10-fold cross
279 validation to calculate test error for each sized model (optimization led to selection of 19 variables out of 27 possible
280 explanatory variables – 7 main and 20 single interactions terms) (Miller, 2020). The model size that minimized test
281 error was selected, and a best-subsets selection method was used to determine the optimal variable coefficients. MLR
282 coefficients from the optimized models were then used to predict nitrite concentration for station depth profiles in the
283 ETNP. Three variations on the 'full' model were made using data from: 1) all stations, 2) a subset of coastal stations
284 (6, 7, 8, and 9) and 3) a subset of offshore stations (13, 14, 15 and 16). Subsets of stations were selected as exemplary
285 of the coastal and offshore regimes based on proximity to the coast, concentration of the chlorophyll maxima, and
286 nitracline depths. The selection criteria for coastal stations used in MLR construction included being close to a
287 coastline, nitracline <40 m depth and chlorophyll maximum larger than 9.5 mg m^{-3} . Offshore stations were selected
288 based on furthest distance from a coastline. Not all stations proximal to the coastline were characterized as coastal
289 (see map) nor included in the 'coastal' subset used to train the model (Table S2a, b).

290 Using the same subsets of ‘coastal’ and ‘offshore’ stations, a second set of MLR models (‘core’ models) was built
291 using a more limited set of core variables from the PPS data that focused on phytoplankton and nitrifier physiology
292 and metabolism (chlorophyll, nitrate, ammonium, oxygen and percent PAR). These five environmental variables, their
293 quadratic terms and single interaction terms were included for 20 parameters in total. This model experiment was
294 constructed to assess the relative importance of these core variables between ‘coastal’ and ‘offshore’ regimes;
295 therefore, no model size optimization was used to limit variables. Instead, optimized coefficients for all variables were
296 determined, and variables that contributed less than 2% of total R^2 in both regional models were discarded. In two
297 cases, a variable that was discarded from one regional model was added back to keep the variable list identical between
298 both models for ease of comparison. For example, in the coastal ‘core’ model, the quadratic term for chlorophyll
299 contributed less than 2% to total R^2 but contributed greater than 2% relative importance within the offshore ‘core’
300 model, and was therefore retained in both models. In the offshore ‘core’ model, PAR was initially removed during the
301 optimization processes because it contributed less than 2% to model R^2 , but was ultimately retained because it
302 contributed greater than 2% relative importance within the coastal ‘core’ model. The relative percent importance of
303 each variable was calculated by iterative random-ordered removal of each variable to estimate percent contribution to
304 total model R^2 using the *relaimpo* package in R (Grömping, 2006).

305 **3 Results**

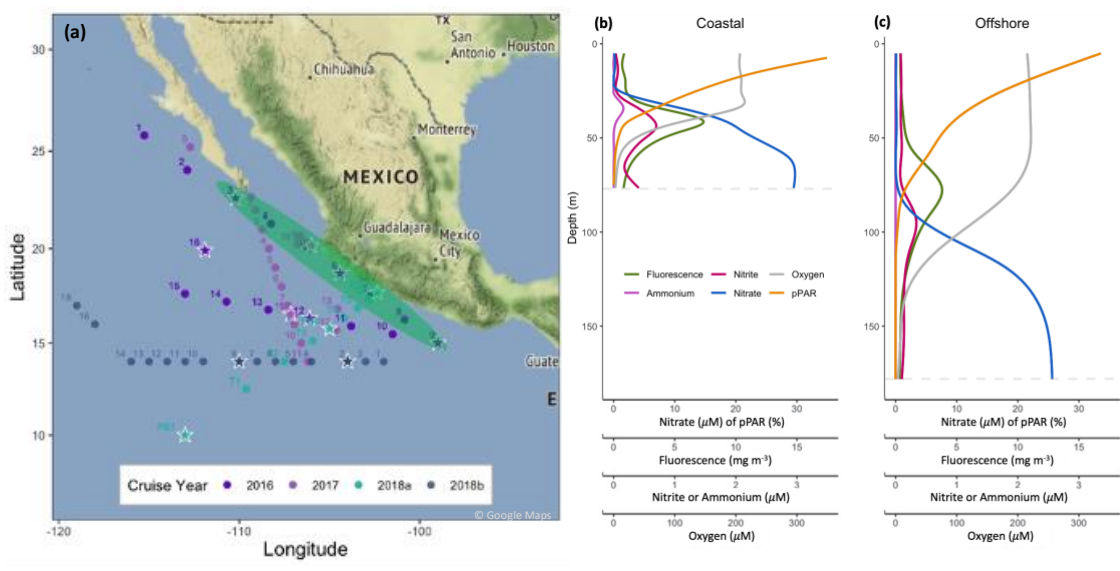
306 **3.1 PNM structure and environmental conditions**

307 The typical PNM feature in the ETNP was a unimodal nitrite accumulation situated just below the chlorophyll
308 maximum and at the top of the nitracline (e.g., Fig. 1b, c). The PNM feature can be described using characteristics of
309 the nitrite profile (i.e., maximum nitrite concentration (μM) and depth of the nitrite maximum (m)) and an integrated
310 nitrite quantity for the whole PNM feature. Although nitrite can seasonally accumulate all the way to the surface in
311 some regions (Zakem et al., 2018), homogenous surface nitrite concentrations were not observed in this dataset. Across
312 the ETNP study region, stations showed similar relative water column structures in the upper 200 m, although the
313 exact depth and magnitude of features varied. Generally, the depth distribution of features from shallowest to deepest
314 was the top of nitracline, the chlorophyll maximum, the ammonium maximum then the nitrite maximum (Fig. 1b, c).
315 This set of sequential features occurred near the base of the euphotic zone at most stations. Surface irradiance
316 attenuated through the water column and the depth of 0.1-1 % surface PAR ranged between 25 m and 150 m depth,
317 with the deepest light penetration at offshore stations. The chlorophyll maximum was usually found around the 1%
318 surface PAR depth and within the nitracline. However, there was variation in how deep the chlorophyll maximum sat
319 within the nitracline, as reflected in the amount of nitrate measured at the depth of the chlorophyll maximum (Table
320 S2a). The depth of the nitrite maximum tended to occur within the downslope of the chlorophyll maximum. The depth
321 horizon of the PNM was often narrow, with detectable nitrite concentrations spanning only 30 m in some cases.

322 The depth of maximum nitrite in the PNM shoaled from an average depth of 103 m at offshore stations to 21 m near
323 the coast, closely following the shoaling nitracline. In density space, the depth of the maximum nitrite fell within a

324 narrower range, from 22.1 to 26.3 kg m⁻³, with a mean density across the study region of 24.1 kg m⁻³. The nitrite
 325 maxima had an average concentration of ~600 nM and a range spanning 60-1520 nM. Two types of stations ('coastal'
 326 and 'offshore') were identified based on water column features. Coastal stations (e.g., 2016 PPS 6, 7, 8, 9) were within
 327 100 miles of the coastline, had higher concentrations of nitrite at the nitrite maxima, shallower depths of the maximum
 328 nitrite, more nitrate and slightly more chlorophyll and light at the depths of the maximum nitrite (Table. S2a). Coastal
 329 stations also had shallower oxyclines, 1% PAR depths, ammonium maxima and chlorophyll maxima compared to
 330 offshore stations. Depth-integrated chlorophyll, nitrate and ammonium in the upper 120 m were higher at coastal
 331 stations. Offshore stations (e.g., 2016 PPS 13,14, 15,16) had deeper nitraclines, smaller chlorophyll maxima and less
 332 light at the depth of the nitrite maxima

333 **Figure 1. Map of the ETNP region showing stations included in this study from four cruises between 2016-2018 (a). Stations**
 334 **where rate measurements were made are marked with white stars. Pump profile data was collected at each station occupied**
 335 **during the 2016 cruise and coastal stations are encircled in green. Mean water column profiles from example 'coastal'**
 336 **stations (8 and 9) and example 'offshore' stations (14 and 16) during the 2016 cruise (b, c). Dashed grey line depicts the**
 337 **depth at which dissolved oxygen concentrations declined below 3 μM.**



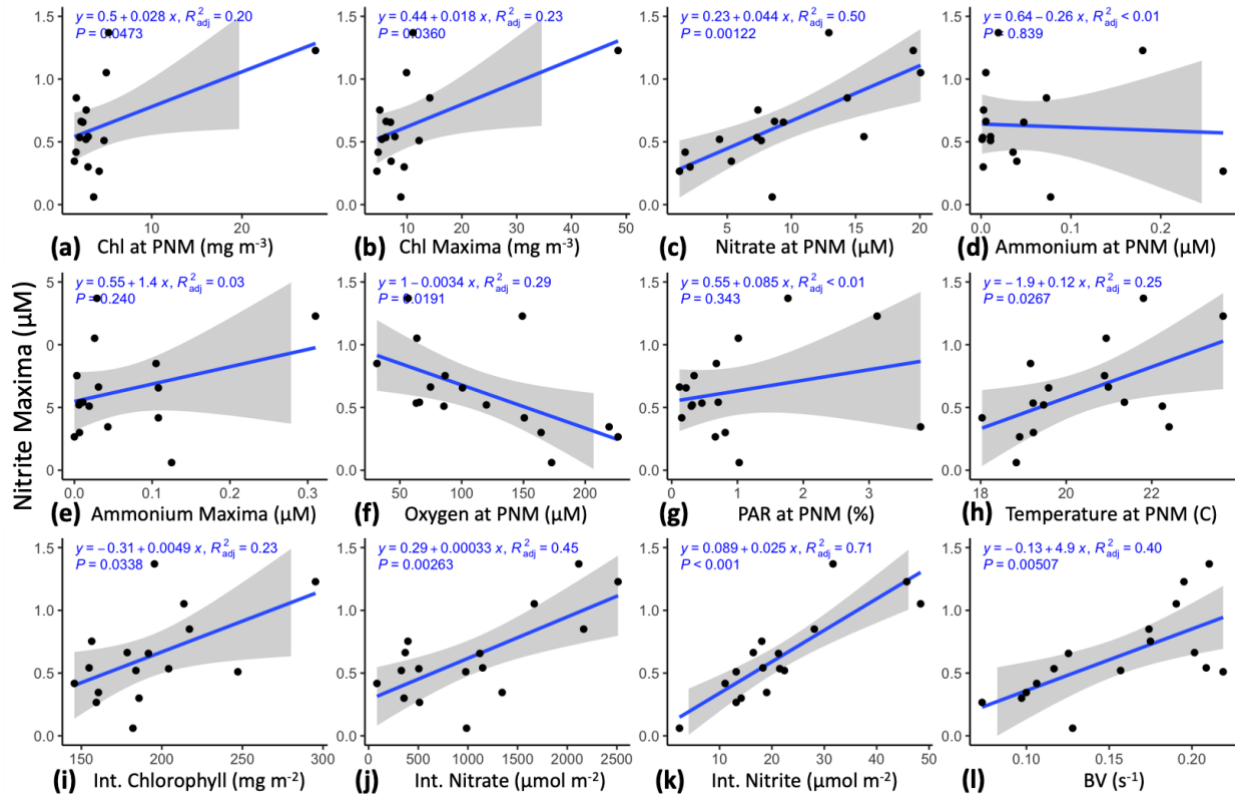
338
 339 **3.2 Regressions with the nitrite maxima**

340 There were no strong linear correlations between the concentrations of nitrite and other observed environmental
 341 variables in vertical profiles (chlorophyll, depth, density, oxygen, temperature, nitrate, ammonium). This is
 342 unsurprising since the variables with unimodal profiles (chlorophyll, ammonium) have concentration maxima that are
 343 offset vertically from the nitrite maximum, and features with other distributions (e.g. exponential) are not expected to
 344 have linear relationships with a unimodal nitrite profile. However, spatial relationships between environmental
 345 gradients are still observed in the quantity regressions; for example, the density regression clearly shows that the peak
 346 of the PNM feature consistently fell near 24 kg m⁻³ isopycnal across the region in 2016.

347 To better match unimodal nitrite profiles with spatially offset and vertically non-unimodal environmental gradients,
 348 station-specific features were identified in the high-resolution 2016 PPS profiles and, where possible, in the CTD

349 datasets (Table 1; e.g., $\text{NO}_2^-_{\text{max}}$ and Z_{NO_2}). The strongest correlation ($R^2 = 0.50$, $p < 0.01$) appeared between $\text{NO}_2^-_{\text{max}}$
 350 (μM) and $\text{NO}_3^-_{\text{pnm}}$ (Fig. 2c). The Brunt-Väisälä frequency (BV), related to water column stability, also had a strong
 351 positive correlation ($R^2 = 0.40$, $p < 0.01$) with $\text{NO}_2^-_{\text{max}}$ (Fig. 2l). There were weaker correlations with other parameters
 352 such as Chl_{pnm} (mg m^{-3}), Chl_{max} (mg m^{-3}), T_{pnm} ($^{\circ}\text{C}$) and $\text{O}_{2\text{pnm}}$ (μM) ($R^2 = 0.20, 0.23, 0.25, 0.29$, respectively, all $p <$
 353 0.05) (Fig. 2a, h, f). Removing the outliers from the two chlorophyll regressions (Fig. 2a, 2b) did not improve the
 354 correlations ($R^2 = 0.06$ and 0.09 , respectively). The $\text{NO}_2^-_{\text{max}}$ was not linearly correlated with PAR_{pnm} (%) or $\text{NH}_4^+_{\text{pnm}}$
 355 (nM) (Fig. 2g, d). The Chl_{Int} , $\text{NO}_3^-_{\text{Int}}$, and $\text{NO}_2^-_{\text{Int}}$ (excluding ODZ waters with $\text{O}_2 < 3 \mu\text{M}$) were higher when
 356 $\text{NO}_2^-_{\text{max}}$ was larger (Fig. 2i, j, k). The $\text{NO}_2^-_{\text{max}}$ had a weak correlation with $\text{NH}_4^+_{\text{Int}}$ (not shown, see Table S2c for
 357 Pearson correlations and p-values). Inclusion of lower resolution CTD casts from cruises in 2017/2018 decreased the
 358 strength of the linear correlations, likely because of larger error in determining the depths of water column features
 359 (e.g., Z_{NO_2} , Z_{nit}) with larger (~ 10 m) spacing between discrete measurements (Fig. S1a).

360 **Figure 2. Linear regressions of $\text{NO}_2^-_{\text{max}}$ against maxima of other parameters, integrated amounts of chlorophyll and DIN,**
 361 **and Brunt-Väisälä frequencies using PPS station data from 2016 (n=16). Chl_{pnm} (a), Chl_{max} (b), $\text{NO}_3^-_{\text{pnm}}$ (c), $\text{NH}_4^+_{\text{pnm}}$ (d),**
 362 **$\text{NH}_4^+_{\text{max}}$ (e), $\text{O}_{2\text{pnm}}$ (f), PAR_{pnm} (g), T_{pnm} (h), Chl_{Int} (i), $\text{NO}_3^-_{\text{Int}}$ (j), $\text{NO}_2^-_{\text{Int}}$ (k), and BV_{pnm} (l). PPS station data from**
 363 **2016 (n=16). Shaded region shows standard error.**



364

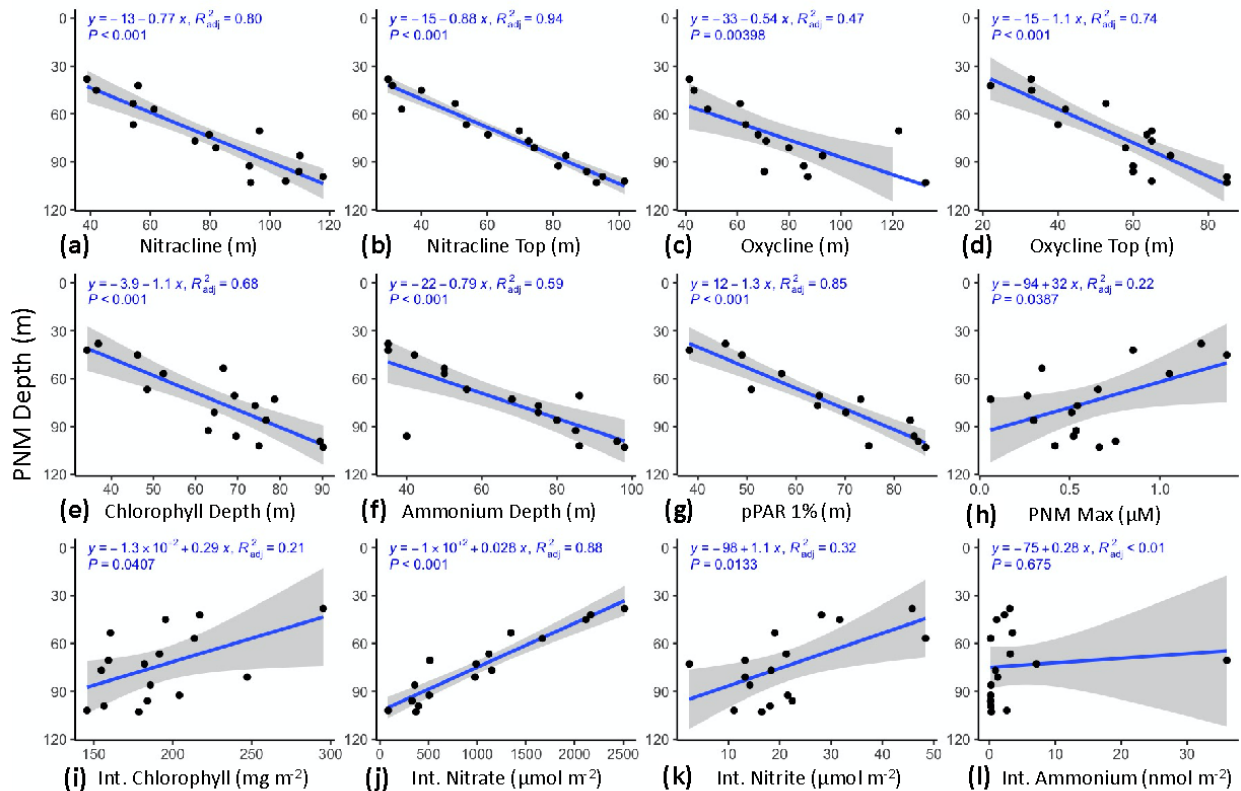
365 3.3 Regressions with depth of the nitrite maxima

366 The depth of the nitrite maximum at each station was also regressed against the depth of station-specific features (Fig.
 367 3). All water column features showed strong linear correlations with the Z_{NO_2} (Fig. 3 a-h). The depth of the (top of the

368 nitracline and Z_{PAR} had the strongest correlations with Z_{NO_2} ($R^2 = 0.94, 0.85$) (Fig. 3b, g). Correlations of Z_{NO_2} with
 369 midpoint-calculated oxyclines and nitraclines were weaker, possibly because those features are less easily defined, or
 370 the steepness of these “clines” were still actively being shaped by the biological responses to changing physical and
 371 environmental forcing. The depth of the nitrite maxima tended to be related to the depths of other features and was not
 372 as strongly correlated with the magnitudes (concentrations) of any other feature (Fig. S2). However, Z_{NO_2} and $NO_2^-_{max}$
 373 were mildly correlated ($R^2 = 0.22, p = 0.039$), with larger $NO_2^-_{max}$ tending to occur at shallower depths. This correlation
 374 became insignificant when the CTD data were included (Fig. S1b). Integrated nitrate had a strong correlation with
 375 Z_{NO_2} ($R^2 = 0.88, p < 0.01$), which is reflective of the depth of $NO_2^-_{max}$ tracking with Z_{nit} . Depth-integrated chlorophyll
 376 and $NO_2^-_{Int}$ had more moderate correlations with Z_{NO_2} ($R^2 = 0.21, p = 0.041$ and $R^2 = 0.32, p = 0.013$, respectively).
 377 Depth-integrated ammonium concentrations did not correlate with the Z_{NO_2} (see Table S2c for Pearson correlations
 378 and p-values).

379 **Figure 3. Linear regression of Z_{NO_2} against water column features from data collected during the 2016 cruise using the PPS.**
 380 **Depth of the nitrite maxima was regressed against: a) Z_{mnit} , b) Z_{nit} , c) Z_{moxy} , d) Z_{oxy} , e) Z_{chl} , f) Z_{NH_4} , g) Z_{PAR} , h) $NO_2^-_{max}$,**
 381 **i) Chl_Int j) $NO_3^-_{Int}$ k) $NO_2^-_{Int}$ and l) $NH_4^+_{Int}$. PPS station data from 2016 (n=16). Shaded region shows standard**
 382 **error.**

383

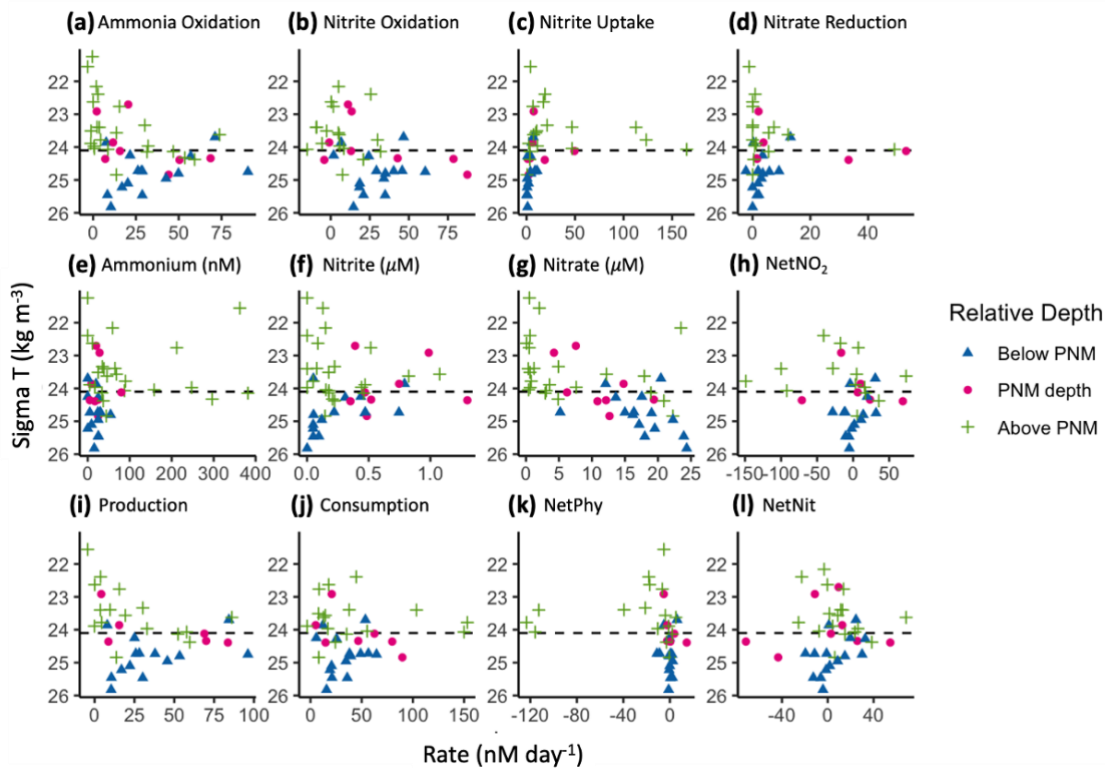


384

385 **3.4 Nitrite Cycling Rates**

386 Rates of nitrite cycling determined for the four major nitrite cycling processes near the PNM were within the same
 387 range as previous measurements made in the ETNP region and along the adjacent California coast (Beman et al., 2008;
 388 Santoro et al., 2010, 2013; Ward et al., 1982). Within our dataset, the mean rates of ammonia oxidation and nitrite
 389 oxidation were similar to each other (24.3 ± 3.6 and 19.5 ± 3.4 nM day^{-1} , respectively), although there was a large range
 390 in individual rate measurements across stations and depths, with maximum rates reaching 90.4 and 87.4 nM day^{-1}
 391 respectively. Rates of the two phytoplankton-dominated processes were generally lower and not as similar to each
 392 other, with a mean nitrate reduction rate of 6.1 ± 1.9 nM day^{-1} and mean nitrite uptake rate of 19.0 ± 5.3 nM day^{-1} .
 393 However, nitrite uptake reached one of the highest rates measured, at 165 nM day^{-1} , and the nitrate reduction rate
 394 reached 53.2 nM day^{-1} at a coastal station during the 2017 winter cruise. Comparison of mean nitrification rates
 395 between coastal and offshore stations did not show a significant difference (Table S1c). The pooled mean standard
 396 deviation across experimental bottle replicates for ammonia oxidation, nitrite oxidation and nitrate reduction were 3,
 397 4.6 and 1 nM day^{-1} , respectively (Table S1).

398 **Figure 4. Aggregated rate measurements from 2016-2018 with respect to density (Sigma T , kg m^{-3}); ammonia oxidation,**
 399 **nitrite oxidation, nitrite uptake and nitrate reduction (panels a-d, respectively) (nM day^{-1}), ammonium (nM), nitrite and**
 400 **nitrate (μM), and net nitrite production (nM day^{-1}) (panels e-h, respectively), and net production, net consumption, net**
 401 **nitrite production from phytoplankton and net nitrite production from nitrification (nM day^{-1}) (panels i-l, respectively).**
 402 **Measurements are colored by relative depth to the station-specific depth of maximum nitrite; above the depth of**
 403 **maximum nitrite (green crosses), at the depth of maximum nitrite (magenta circles) or below the depth of the maximum**
 404 **nitrite (blue triangles). The mean isopycnal (24.1 kg m^{-3}) for the ETNP nitrite maxima is marked as a horizontal dashed**
 405 **line.**



406

407 When plotted in density space to aggregate data across years and stations, all processes showed rate maxima at a
408 subsurface density layer (Fig. 4). Nitrifier processes (ammonia oxidation (Fig. 4a) and nitrite oxidation (Fig. 4b)), had
409 maximal rates near, or just below, the average density layer for the nitrite maxima across this region (24.1 kg m^{-3}).
410 Nitrite uptake (Fig. 4c) and nitrate reduction (Fig. 4d) rates reached their maxima just above the mean nitrite maxima
411 isopycnal. Nitrification rates were highest in the lower half of the nitracline, while phytoplankton-dominated processes
412 (nitrite uptake and nitrate reduction) were highest on the upper slope of the nitracline where light was available and
413 nitrite and ammonium concentrations were higher. While the highest activities of the two microbial groups were
414 spatially segregated, within-group production and consumption processes had maxima at similar depths. All four rates
415 formed vertically unimodal distributions, but there was still a large range in measured rates near the peaks with many
416 rates close to zero.

417 Net nitrite production from nitrification ($\text{NetNit} = \text{ammonia oxidation} - \text{nitrite oxidation}$) ranged from -71.5 to 68.4
418 nM day^{-1} with a mean of $5.6 \pm 3.6 \text{ nM day}^{-1}$ (Fig. 4I). The majority of NetNit values were positive, and maximal rates
419 were observed just below the mean nitrite maxima isopycnal. Negative NetNit values were driven by high nitrite
420 oxidation values. Net nitrite production from phytoplankton-dominated processes ($\text{NetPhy} = \text{nitrate reduction} - \text{nitrite}$
421 uptake) were typically low (mean $-13.3 \pm 4.9 \text{ nM day}^{-1}$), with many negative values resulting from rates of nitrite uptake
422 exceeding those of nitrate reduction (Fig. 4k). The largest negative values occurred above the mean nitrite maxima
423 isopycnal, driven by high nitrite uptake rates where light concentrations were high and nitrate was low in the surface
424 waters. Below the mean nitrite maxima isopycnal, NetPhy remained near zero because both nitrite uptake and nitrate
425 reduction rates were low. The largest positive NetPhy value was at a coastal station (14.4 nM day^{-1}), where nitrate
426 reduction reached 33.1 nM day^{-1} , but NetPhy was typically an order of magnitude smaller than NetNit .

427 The vertical distributions of total nitrite production (production = ammonia oxidation + nitrate reduction, Fig. 4i) and
428 total nitrite consumption (consumption = nitrite oxidation and nitrite uptake, Fig. 4j) showed maximal rates near the
429 mean nitrite maxima isopycnal (24.1 kg m^{-3}). Total nitrite production peaked just below this, with a maximum value
430 of 87 nM day^{-1} . Total nitrite consumption peaked just above it, with a maximum value of 167 nM day^{-1} . The higher
431 consumption rates just above the mean nitrite maxima isopycnal were due to higher nitrite uptake rates, especially at
432 coastal stations (Fig. 4c). There was a large range in rates of nitrite production and consumption processes, but mean
433 values were of similar magnitude (26.4 nM day^{-1} and 39 nM day^{-1} , respectively). Total net nitrite production (NetNO_2 ,
434 the difference between total production and total consumption) was highest near the PNM. Negative net nitrite
435 production rates could be found both above and below the PNM, reflecting high nitrite uptake above the mean nitrite
436 maxima isopycnal and high nitrite oxidation values below it (Fig. 4h). The mean of positive NetNO_2 values was 16.7
437 nM day^{-1} (rates > -2 only, $n=17$), although mean NetNO_2 was -6.3 nM day^{-1} when all data points were included. The
438 maximum rate of NetNO_2 was slightly higher than NetNit (73.5 vs 68.4 nM day^{-1} , respectively), but the peaks of the
439 vertically unimodal distributions occurred at the same depths.

440 While the aggregated rates of NetNO_2 peaked near the mean nitrite maxima isopycnal for the region, neither NetNO_2
441 (nor any individual rates) were able to predict the observed nitrite concentrations. Simple linear regressions of each

442 rate, or calculated net rates, against the quantity of nitrite did not show significance (Fig. S4). Limiting the regression
443 to a single nitrite maximum and a single highest rate per station also did not show any linear correlation (Fig. S5).
444 However, some qualitative patterns were noticeable, where the highest rates of phytoplankton-dominated processes
445 occurred in samples with lower nitrite concentrations (shallower in the water column). The highest nitrite uptake rates
446 ($>25 \text{ nM day}^{-1}$) appeared to co-occur with maximum nitrite concentrations below 500 nM. Conversely, when high
447 nitrite concentrations were measured ($>600 \text{ nM}$), nitrite uptake rates were low (never higher than 10 nM day^{-1}). Nitrate
448 reduction rates were also higher at lower nitrite concentrations. In addition, the highest ammonia oxidation rates (>40
449 nM day^{-1}) were found where nitrite concentrations were $<500 \text{ nM}$ (Fig. S4). Interestingly, nitrite concentrations were
450 highest ($>600 \text{ nM}$) where ammonia oxidation rates were lower ($<40 \text{ nM day}^{-1}$). The highest nitrite concentrations were
451 associated with waters having lower nitrite oxidation rates ($<20 \text{ nM day}^{-1}$), indicating a low rate of nitrite consumption.
452 Thus, although nitrification was an important contributor to total nitrite production, the balance of processes was more
453 important than the rate of any single process.

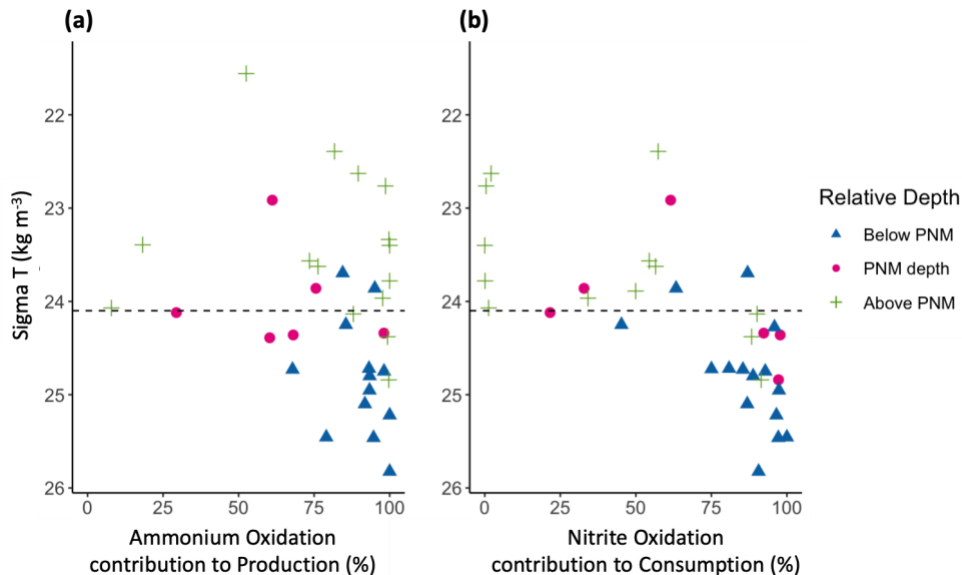
454 If we assume approximate steady state for PNM nitrite concentrations, rate measurements can be used to calculate a
455 potential residence time for nitrite across the PNM feature. Using total nitrite production and nitrite concentrations,
456 the mean residence time was 30.4 days, while the median residence time was 7.8 days. However, there was a wide
457 range in residence times across all samples, particularly those from above the average nitrite maxima isopycnal for
458 the region (Fig. S6a). Using total consumption rates in the calculation gave a slightly lower mean residence time for
459 the region (20.3 days), but again had a large range in residence times above the mean nitrite maximum isopycnal
460 (0.01-103.2 days) (Fig. S6c). Our estimates of average residence time using potential rates may be underestimated
461 because of rate enhancement from tracer additions, and we are also likely missing an input/output term from physical
462 mixing, which could have a larger influence in dynamic coastal waters compared to offshore. Comparing coastal and
463 offshore stations, the estimated residence times are quite different between regimes (mean residence times of 17 and
464 53 days, respectively, and median residence times of 5.8 and 18.2 days, respectively) suggesting that coastal nitrite
465 accumulations are turning over more quickly even with the limitations and assumptions of these calculations. The
466 discrepancy in residence times calculated using the influx and outflux terms for the nitrite pool suggests that the PNM
467 feature was most likely not in steady state (as also suggested by the high variation in measured rates across the PNM
468 and inability of rates to correlate with observed nitrite accumulation), with differences in the dynamics above and
469 below the nitrite maxima. Additional methods of estimating nitrite age, such as using variation in natural abundance
470 nitrite isotopes, may provide more insight (Buchwald and Casciotti, 2013).

471 **3.5 Contribution from Nitrification**

472 In considering the metabolisms responsible for accumulation of nitrite at the PNM, it is important to consider the
473 distribution and magnitude of nitrite production processes vertically through the water column as well as their relative
474 contributions to total nitrite production. At our sites in the ETNP, ammonia oxidation contributed over 70% of the
475 total nitrite production through most of the water column (Fig. 5a). The stations where ammonia oxidation contributed
476 less to total nitrite production were typically coastal stations with low ammonia oxidation rates (e.g., $<2 \text{ nM day}^{-1}$) or

477 with high nitrate reduction rates ($>20 \text{ nM day}^{-1}$). These results support the idea that both ammonia oxidation and nitrate
 478 reduction can contribute to nitrite production, but show that the dominant source was ammonia oxidation at most
 479 stations, particularly at the depth of the nitrite maximum and below. For nitrite consumption, nitrite oxidation
 480 contributed greater than 70% of total nitrite consumption below the mean density layer of the nitrite maxima. Above
 481 this density layer, the contribution to total nitrite consumption from nitrite oxidation became more variable, but with
 482 most values below 70% due to more nitrite uptake. Particularly low contributions to total nitrite consumption from
 483 nitrite oxidation were seen above the depth of the nitrite maxima at coastal stations where nitrite uptake rates were
 484 highest. Potential decoupling of ammonia and nitrite oxidation could be seen in the upper water column, with NetNit
 485 peaking at the depth of the nitrite maxima (Fig. 4I), which is more difficult to discern in the individual ammonia
 486 oxidation and nitrite oxidation rates (Fig. 4a, b).

487 **Figure 5. Contributions of nitrification to total nitrite production (a) and total nitrite consumption (b) across density space.**
 488 **Measurements are colored by depth relative to the station-specific depth of maximum nitrite; above the depth of maximum**
 489 **nitrite (green crosses), at the depth of maximum nitrite (magenta circles) or below the depth of maximum nitrite (blue**
 490 **triangles). The mean ETNP nitrite maxima isopycnal (24.1 kg m^{-3}) is marked as a horizontal dashed line**



491

492 3.6 Multiple Linear Regression Analyses

493 3.6.1 'Full' model PNM predictions

494 Multiple linear regression analyses using all available variables (i.e. the "full" model) was able to predict the presence
 495 of a PNM at most stations when trained using all stations, the coastal station subset, or the offshore station subset (Fig
 496 S3). However, variables selected during optimization and the coefficients determined were not consistent across the
 497 three full models, and depth and size accuracy of nitrite predictions was highly variable (Table S3, S4).

498 The all-station 'full' model predicted the depth of the maximum nitrite well (mean depth error = 3.7 m) but
 499 underpredicted the concentration of the nitrite maxima by an average of 230 nM across all stations (after the extreme

500 over-prediction of 15 μM at Station 8 was omitted) (Fig. S3, Table S4). Retraining the model using a subset of coastal
501 stations improved fit for the training subset of stations (mean depth error 2.9 m), but was no longer applicable across
502 other stations in the region (Fig S3). When applied to non-coastal stations, the coastal ‘full’ model overpredicted ($>2x$)
503 the concentration of the nitrite maxima (except Stations 10,11,12), with an average overprediction for the whole region
504 of $\sim 1.13 \mu\text{M}$ (Table S4). Similar results were found when the model retrained using the offshore subset of station.
505 The offshore ‘full’ model predicted the depth of maximum nitrite well for offshore stations, with a mean
506 underprediction in depth of only 0.3 m (Fig. S3, Table S4), and underpredicted the concentration of the nitrite
507 maximum at offshore stations by only 53 nM on average. The mean overprediction of nitrite concentration by the
508 offshore ‘full’ model applied across all stations was 855 μM , driven by an extreme overprediction at Station 8, which
509 when excluded, makes the mean size error only 1.23 μM .

510 This set of ‘full’ variable models showed that there is enough information in the environmental data to make
511 correlative predictions of nitrite profiles, but also showed regional variability precludes a single model for the region.
512 Additionally, investigating model variables and coefficients to gain insight on environmental controls of the PNM is
513 difficult when different variables are used in each version of the model.

514 **3.6.2 ‘Core’ model PNM predictions**

515 A subset of ‘core’ variables was selected and applied in a second set of MLR analyses in order to directly compare the
516 influence of each variable on nitrite concentration between two regions (coastal vs. offshore) (See Methods). The ‘core’
517 models limited variables to those that had strong single linear regressions with depth and concentration of the nitrite
518 maxima, and both the coastal and offshore models explained similar amounts of the total variance in nitrite
519 concentration in their respective regions. Even though both models explained relatively similar amounts of variation
520 in nitrite concentration and used the same limited suite of variables, different coefficients led to differing predicted
521 nitrite profiles across stations (Fig. 6, Table 2). In the coastal region, the primary model components included nitrate
522 and light, two environmental variables that are related to initiation of bloom conditions. The offshore model shifted
523 importance slightly towards a stronger chlorophyll component and reduced the importance of light. In both regional
524 models, nitrate was involved in explaining the most variance (40.8% in the coastal model, 38.8% in the offshore
525 model).

526 **Table 2. Coefficients and relative importance from core models; coastal (a) and offshore (b)**

(a)

Coastal 'Core' MLR Coefficients		
Variable	Coefficient	Percent Importance
Oxygen-Nitrate	0.0028	18.9
Nitrate	-0.4137	12.2
pPAR	-0.0183	12.1
Chl-Nitrate	0.0538	9.7
Chlorophyll	-0.0837	4.6
Oxygen	-0.0047	4.6
Chlorophyll2	-0.0014	2.3

(b)

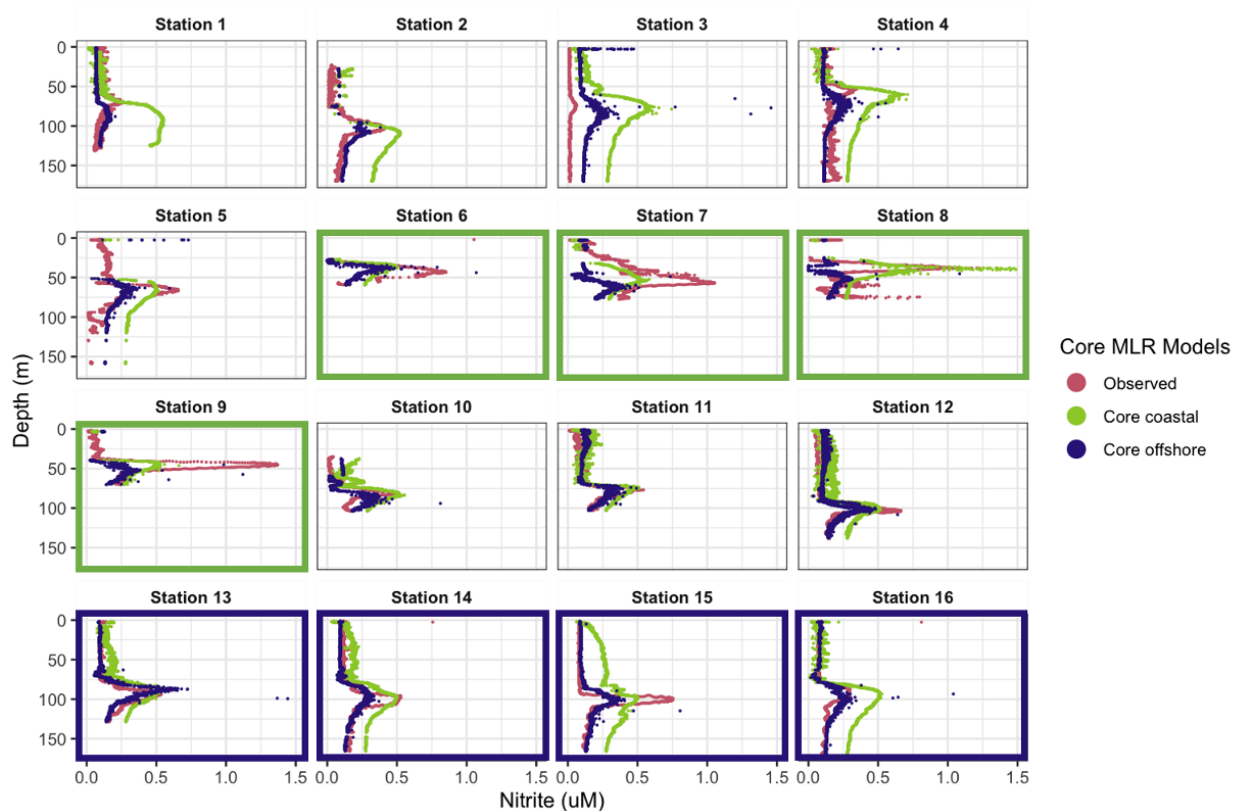
Offshore 'Core' MLR Coefficients		
Variable	Coefficient	Percent Importance
Chl-Nitrate	0.0752	16.7
Oxygen-Nitrate	0.0029	11.9
Chlorophyll	0.46	11.1
Oxygen	-0.0124	11
Nitrate	-0.7093	10.2
Chlorophyll2	-0.0994	6.8
pPAR	-0.0012	4.4

527
528 In general, the coastal 'core' model predicted the depth of the PNM well, but was less accurate in predicting maximum
529 nitrite concentration, and peak shape (Fig. 6). The coastal 'core' model underpredicted the depth of the nitrite maxima
530 at coastal stations (-1.7 m), and underpredicted coastal nitrite maxima by an average of 208 nM, with a large range in
531 error (-830 to +811 nM) (Table S5). Applying the coastal model to the full set of 16 stations showed that the coastal
532 'core' model could either overpredict or underpredict the concentration of the nitrite maxima at non-coastal stations,
533 in addition to predicting a wide PNM shape that extends deeper in the water column than observed (Fig. 6). The
534 predicted depths of the nitrite maxima from the coastal model fit well with the depths of the observed nitrite maxima,
535 with a mean depth overprediction of only 2.3 m; a single large outlier at Station 1 was observed, where PNM depth
536 was overpredicted by 23.4 m (Fig. 6, Table S5).

537 The offshore 'core' model also predicted the depth of the nitrite maxima well, but less accurately predicted the
538 concentration of the nitrite maxima (Fig. 6). The depths of the nitrite maxima at offshore stations were predicted to
539 within 2.8 m, but concentrations of the nitrite maxima were underpredicted by 82 nM at offshore stations. Applying
540 the offshore core model across all 16 stations showed that it worse on average, giving predicted depths of maximum
541 nitrite that were on average 5.5 m deeper than the observed depth, with a range in over- and underpredictions from
542 18.6 m to 5.5 m respectively. The predicted concentrations of nitrite maxima were lower than observations by an
543 average of 218 nM across the region (Table. S5).

544 **Figure 6. Predicted nitrite profiles from 'core' coastal MLR (green) and offshore MLR (blue). Observed nitrite profiles**
545 **from PPS 2016 dataset (magenta). Panels of stations used to train the coastal model are traced in green, and panels for**
546 **stations used to train the offshore model are traced in blue.**

547



548

549

550 **4 Discussion**

551 **4.1 Vertical structure of nitrite accumulation**

552 The same vertical sequence of water column features was seen at all ETNP stations, with the chlorophyll maximum
 553 lying above the ammonium maximum lying above the depth of the nitrite maximum at the top of the nitracline. These
 554 consistent spatial relationships between water column features suggest that there is a specific set of environmental
 555 conditions and biological agents that lead to the accumulation of nitrite. Linear regressions between depth of the nitrite
 556 maxima and the depth of other key water column features indeed showed strong correlations. Previous work has noted
 557 the connection of the depth of the nitrite maximum with the nitracline (Dore and Karl, 1996; Herbland and Voituriez,
 558 1979; Lomas and Lipschultz, 2006; Meeder et al., 2012; Shiozaki et al., 2016; Vaccaro and Ryther, 1960) and with
 559 the chlorophyll maximum (Collos, 1998; French et al., 1983; Kiefer et al., 1976; Meeder et al., 2012), showing that
 560 these relationships are shared across multiple oceanic regimes. The environmental feature that correlated most strongly
 561 with the depth of the nitrite maximum in our dataset was the top of the nitracline, while the depth of the chlorophyll
 562 maximum, the depth of the ammonium maximum, the depth of 1% PAR and the top of the oxycline also showed
 563 strong correlations, as illustrated by regression analysis (Fig. 3).

564 The strong covariance between multiple features provides some insight into the mechanisms that link the depth of the
 565 nitrite maximum to the environment. Nitrite-cycling microbes respond to the differences in environmental conditions

566 above and below the PNM. In oligotrophic waters, such as those in the offshore ETNP, uptake of nutrients by
567 phytoplankton maintains low levels of DIN in the upper euphotic zone as physical resupply is low. As light decreases
568 with depth in the water column, active phytoplankton growth is diminished and ammonium and labile dissolved
569 organic nitrogen are released due to grazing and decomposition, providing the low-light conditions, ammonium and
570 reduced organic N substrates suitable for ammonia oxidation. Nitrite oxidizers utilize nitrite produced predominantly
571 from ammonia oxidation to return nitrate to the system. Above the PNM, where light is available, there is enhanced
572 potential for nitrite uptake by phytoplankton and nitrite does not accumulate. Below the PNM, there is diminished
573 supply of ammonium and nitrite oxidizers continue to consume low levels of nitrite produced through ammonia
574 oxidation. At the depth of the nitrite maximum, production terms outweigh both spatially segregated loss terms—
575 nitrite uptake and nitrite oxidation.

576 The production of nitrite at the PNM is linked to the vertical structuring of the upper water column qualities and is
577 both directly and indirectly dependent on phytoplankton activity. It is directly related via the potential for
578 phytoplankton to release nitrite under varying nitrate supply and light conditions, and indirectly through ammonium
579 supply provided to the ammonia-oxidizing community. Interestingly, the sequence of events that structures the
580 nitracline at the base of the euphotic zone (nitrate and light availability → uptake of nitrate and phytoplankton growth
581 → formation of the nitracline and oxycline = release of ammonium (and nitrite) → oxidation of ammonium by
582 nitrifiers) is ordered similarly to the strength of the linear relationships with the depth of maximum nitrite (top of
583 nitracline > %PAR > chlorophyll/ oxycline > ammonium peak depth). The physical processes that change light and
584 mixing environments initiate the conditions under which phytoplankton and nitrifiers establish their contributions to
585 the PNM over time. The importance of the time component may help explain why there is variation in the strength of
586 correlation between instantaneous environmental measurements and a PNM structure that may require weeks to form.
587 Under more dynamic conditions (e.g., coastal upwelling), our observations are more likely to capture a larger range
588 in scenarios, from initial upwelling to cessation of upwelling, making correlations between the depth of maximum
589 nitrite and other water column features weaker.

590 **4.2 Concentration of the nitrite maximum**

591 While the depth of maximum nitrite is predictable based on features of the water column, the concentration of the
592 nitrite maximum was more challenging to predict. In regressions of water column features against the concentration
593 of the nitrite maximum, only the amount of nitrate at the nitrite maximum, the Brunt-Väisälä frequency and the amount
594 of oxygen at the nitrite maximum had moderate linear relationships ($R^2=0.5$, $p < 0.01$, $R^2 = 0.4$, $p = 0.016$, $R^2 = 0.29$,
595 $p = 0.019$), while the R^2 values for the other regressions were smaller ($R^2 < 0.25$) (Fig. 2). The connection between the
596 nitrite maximum and nitrate concentration may reflect the sequence of events that structures the water column and
597 forms the nitracline (described above). The presence of increased amounts of nitrate at the depth of larger nitrite
598 maxima suggests that the phytoplankton have yet to deplete nitrate completely, and a large nitrite maximum is
599 developing during active nitrate uptake at early bloom formation (Collos, 1982; Meeder et al., 2012). At stations with
600 a large nitrite maximum, there are also higher concentrations of nitrate at the chlorophyll maximum, although the

601 chlorophyll maximum may still be small (i.e., early bloom). During this time, ammonium production from degrading
602 and grazed phytoplankton as well as ammonia oxidation to nitrite may co-occur. Under these early bloom conditions
603 there is potential to accumulate more nitrite due to increased rates of phytoplankton nitrate reduction, high rates of
604 ammonia oxidation, and/or decrease in loss terms. Controls on nitrate reduction rate, and the potential for ammonium
605 competition interactions between phytoplankton and ammonia oxidizers at nitrate replete depths will be discussed in
606 relation to nitrite cycling rates.

607 The linear correlation between the larger nitrite maxima and stronger density gradients (higher Brunt-Väisälä values)
608 suggests that decreased loss of nitrite via mixing could contribute to larger accumulation of nitrite at the maximum.
609 However, degradation of the nitrite maximum by mixing would only move existing nitrite away from the peak depth,
610 not remove it entirely from the water column.

611 We took two further approaches to understand the correlative disconnect between environmental conditions and nitrite
612 maxima, 1) polynomial multiple regression analyses which allow multiple variables to co-explain the depth and
613 concentration of the nitrite maxima, and 2) making direct measurements of the microbial processes that
614 mechanistically link environmental conditions to the nitrogen transformation rates leading to nitrite accumulation.

615 **4.3 Predicting nitrite profiles from environmental dataset**

616 The lack of strong linear correlations between maximum nitrite concentrations and any single feature may indicate
617 that multiple conditions need to be met to produce large accumulations of nitrite. For example, earlier work has shown
618 the largest seasonal nitrite maxima occur at the onset of the deep chlorophyll maximum, where multiple conditions
619 are met— light is available and nitrate concentrations are still high (Mackey et al., 2011; Meeder et al., 2012).

620 Allowing for multiple environmental conditions to contribute, the ‘full’ multilinear regression models are qualitatively
621 able to capture the peak shape of the PNM feature using the variables provided, yet are unable to fully explain nitrite
622 concentration (Fig. S3). For example, the all-station ‘full’ model explained 66% of the overall variance in nitrite
623 concentration, but the mean error in nitrite maximum predictions was 740 nM with a large range in errors across
624 stations (-0.84 to 15.28 μM) (Table S4). This large uncertainty is not surprising, since environmental conditions vary
625 across the ETNP, especially between coastal and offshore stations. The coastal and offshore nitrite maxima were
626 typically found at similar densities ($\sim 24.1 \text{ kg m}^{-3}$), but at coastal stations the average depth of the nitrite maxima was
627 43 m shallower, the average nitrate concentration was 3x higher, the average chlorophyll concentration was 3x higher,
628 average light was 3x higher, oxygen was 25% higher and ammonium concentrations were also higher (Table S2). This
629 suggests that the nitrite maxima at coastal and offshore type stations may be innately different, and possibly controlled
630 by a different balance of mechanisms. The two ‘full’ models built using coastal and offshore subsets were able to
631 explain more of the total variance at those stations ($R^2 = 0.77$ and 0.79 , respectively).

632 The ‘core’ models, where the variables included in the models were consistent between the coastal and offshore
633 regimes, were also able to explain a significant portion of the variability in nitrite (R^2 was 0.83 and 0.98 , respectively).

634 Nitrate was a key parameter in both models (Table 2). The smaller chlorophyll coefficients used to model nitrite
635 maxima at coastal stations make the model less sensitive to large changes in chlorophyll, while the larger offshore
636 coefficient suggests that small changes in chlorophyll offshore have more influence over the resulting nitrite
637 predictions. While there was still significant error in the predicted depth and concentration of the nitrite maxima, the
638 'core' model coefficients show patterns suggesting that nitrite accumulation occurs at depths where chlorophyll, nitrate
639 and oxygen co-exist, corroborating the findings from that linear regression analyses, that the depth of the chlorophyll
640 maxima, nitracline top and oxycline top are individually important in determining the depth of the nitrite maximum
641 (see Supplement for further comparison of coefficients).

642 Overall, while the nitrite accumulation in the PNM was predicted moderately well using the environmental conditions,
643 especially when differentiating between coastal and offshore regimes, the environmental parameters alone were not
644 able to fully predict nitrite concentrations. Variable physiological responses of the microbial populations involved
645 with nitrite production and consumption provide a mechanism that integrates multiple environmental parameters into
646 an observable nitrite accumulation.

647 **4.4 Rates of Nitrite Cycling**

648 Strong single variable correlations with depth of the nitrite maxima and mild correlations with concentration of nitrite
649 at the nitrite maxima (with supportive findings from the MLR analyses), suggest that while the PNM feature is
650 consistently linked to specific depths, the maximum concentration of nitrite in a given PNM may be modulated by
651 more nuanced environmental timings and microbial physiologies. The two main biological mechanistic explanations
652 for nitrite production at the PNM involve the microbial physiology of phytoplankton and nitrifying bacteria and
653 archaea. The overlapping habitats and competition for DIN resources requires that we consider both microbial groups
654 in our understanding of PNM formation (Lomas and Lipschultz, 2006; Mackey et al., 2011; Smith et al., 2014; Wan
655 et al., 2021, 2018; Zakem et al., 2018). This dataset provides insights into the relative roles of these processes via
656 direct rate measurements of the four major nitrite cycling processes from the same source water. This allows both
657 comparison of relative rates of each process within a community and the calculation of net rates of nitrite production
658 around the PNM feature. Our expectation at the beginning of this study was that higher rates of nitrite production, or
659 net nitrite production, would correspond to larger accumulations of nitrite. Our findings, however, revealed a more
660 complex pattern where the instantaneous rates of gross or net nitrite production did not reflect the amount of
661 accumulated nitrite. In other words, the imbalance in nitrite production and consumption can indicate whether nitrite
662 concentrations are currently increasing or decreasing, but it provides less predictive power for the concentration of
663 accumulated nitrite. Some of the discrepancy between rates and observed nitrite accumulation may also be attributable
664 to potential enhancement of rates from tracer addition, or nitrite production from other sources not captured in our
665 tracer experiments.

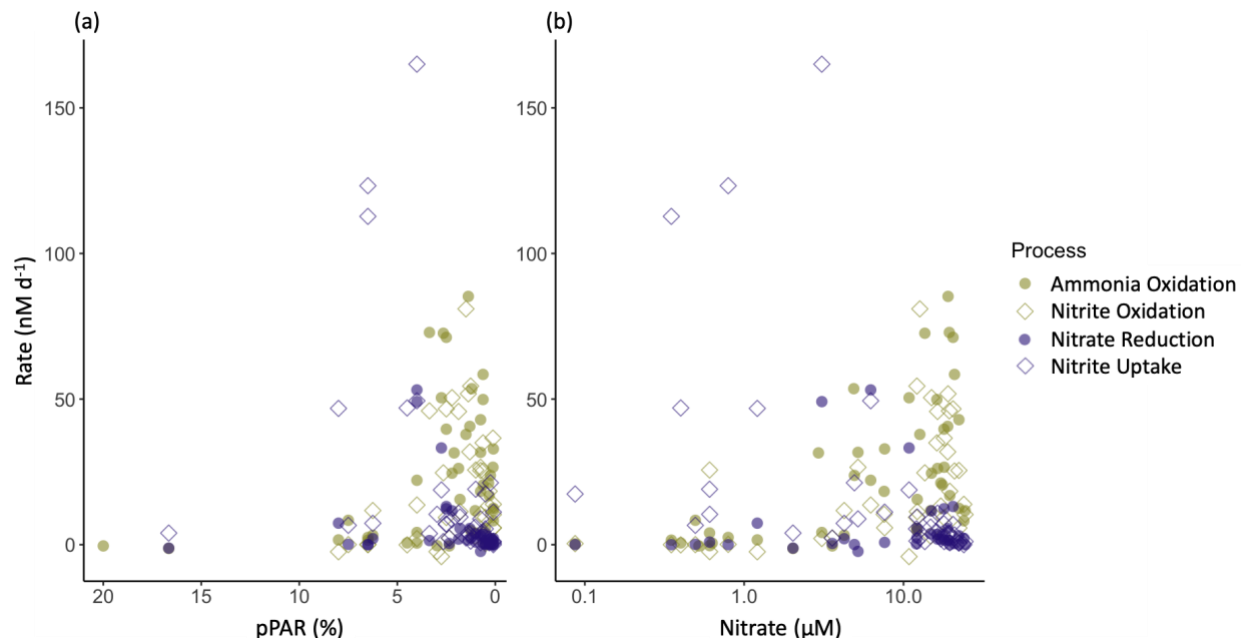
666 The spatial distribution of measured rates through the water column showed peaks in each process near the PNM, but
667 with slight variation in where the rate maxima fell relative to the nitrite maxima. The highest phytoplankton activity
668 was located just above the PNM peak, while nitrification rates were highest near the PNM peak, a distribution seen in

669 other nearby systems (Beman et al., 2012; Santoro et al., 2013). Although the aggregated data from the region showed
670 these spatial segregations by microbial group, this was not always observed at an individual station. The highest rates
671 of nitrification appear to be slightly skewed towards the lower slope of the PNM, but the depth of the nitrite maximum
672 at many stations was determined from discrete measurements taken at ~10 m resolution, so it is possible that the real
673 maxima occurred between sampled depths. The PPS data allowed much more precise determination of the depth and
674 peak size, although rate measurements were still limited to lower resolution sampling.

675 The vertical distribution of nitrification has been theorized to be controlled by light inhibition, restricting nitrification
676 to depths at the base of the euphotic zone (Olson, 1981). However, active nitrification has been observed in the sunlit
677 surface ocean (Shiozaki et al., 2016; Ward, 2005; Ward et al., 1989), leading to new theories suggesting that ammonia
678 oxidation is controlled by ammonium or nitrate availability shifting the competitive balance for ammonium acquisition
679 away from phytoplankton and towards ammonia oxidizers (Smith et al., 2014; Wan et al., 2018; Xu et al., 2019). In
680 this dataset, we did measure nitrification rates $>2 \text{ nM day}^{-1}$ at light levels of 25-30% surface PAR at coastal stations,
681 although there was a clear enhancement of nitrification rates at light levels below 5% surface PAR. Although linear
682 regressions of ammonia oxidation rate didn't show a strong correlation with the nitrite maximum or the depth of
683 maximum nitrite, there was a relationship between ammonia oxidation and both nitrate and light (Fig. 7). Similar to
684 the data compiled in Wan et al. (2018), the highest ammonia oxidation rates were restricted to depths with higher
685 nitrate concentrations and lower light levels. However, even when constraining the ammonia oxidation rate data to
686 where there is both low light and higher nitrate concentrations, measurements spanned the entire range of rates from
687 0-85 nM day^{-1} , indicating that the conditions controlling the depth of the rate maxima do not guarantee high rates, but
688 simply facilitate the possibility of high rates. It should be noted that some of the highest rates were measured in source
689 water with low ambient DIN concentrations, and it is possible that tracer addition relieved DIN-limitation in some of
690 these samples and enhanced the measured rates (Fig S7). However, as these are bulk rates (per volume), we cannot
691 differentiate between potential enhancement of rates due to our tracer addition versus different microbial abundances.

692

693 **Figure 7 Relationship between nitrite cycling rates and percent surface PAR (a) and nitrate concentration (b).**
694 **Phytoplankton-dominated processes are shown in purple and nitrifier processes are shown in green. Nitrite production**
695 **processes are shown as filled circles and nitrite consumption processes are open diamonds.**



696

697 The individual rate measurements were not correlated with the amount of nitrite accumulated in the water column at
 698 a given depth (Fig. S4). Neither were the net rates (NetNit, NetPhy, NetNO₂) able to explain observed nitrite
 699 concentrations. Although the vertical pattern in net nitrite production rates (NetNO₂) showed a peak shape that was
 700 qualitatively similar to nitrite concentration, there was no linear relationship between NetNO₂ and nitrite
 701 concentration (Fig. 4h, Fig. S4), suggesting that instantaneous rate measurements do not always represent time
 702 integrated nitrite accumulation in the PNM. Because our measurements were of whole community rates, a variety of
 703 microbial processes may have remained active in the incubations alongside the process intended to be traced with
 704 ¹⁵N. For example, the ¹⁵N-NO₂⁻ produced via nitrate reduction is potentially acted upon by nitrite uptake and nitrite
 705 oxidation. This has the potential of leading to underestimation of nitrate reduction rates, especially where nitrite
 706 concentrations are low, and nitrite uptake and nitrite oxidation rates are large.

707 Nitrification rates were similar in magnitude between coastal and offshore stations (Table S2), with the major
 708 differences in rate measurements between coastal and offshore stations found in the phytoplankton-dominated
 709 processes (nitrate reduction and nitrite uptake). The highest rates of phytoplankton activity were found at coastal
 710 stations and occurred primarily above the depth of the PNM. The distribution of measured activity lends support to
 711 the hypothesis that phytoplankton may outcompete nitrifiers for DIN sources above the nitrite maximum (Wan et al.,
 712 2018; Zakem et al., 2018). This proposed mechanism accounts for the correlations seen between lower light levels and
 713 higher ammonia oxidation because the top of the nitracline itself is a physical demarcation of the depth where
 714 phytoplankton co-requirements for light and nitrate are met. Previous work has also shown that the presence of nitrate
 715 can inhibit nitrite uptake by phytoplankton through competitive interactions (Eppley and Coatsworth, 1968; Raimbault,
 716 1986) (Fig. 7b). This mechanism may provide a way to connect the presence of nitrate with a larger PNM that relies
 717 on prevention of nitrite loss, rather than an increase in nitrite production.

718 An additional loss term that could influence the size of the observed nitrite peak is diffusion, moving nitrite away from
719 the depth of maximal net nitrite production. In addition to having shallow nitraclines and shallow chlorophyll
720 maximum depths, as well as larger chlorophyll maxima and nitrite maxima, coastal stations also had the steepest
721 density gradients near the PNM, making Brunt-Väisälä (BV) frequency correlate with the nitrite maxima in this dataset
722 ($p=0.005$) (Fig S9, Fig. 2I). The strong density gradients at the coastal stations (stations 6, 7, 8, 9) would inhibit mixing,
723 potentially allowing for larger concentrations of nitrite to accumulate for a given rate of net nitrite production. This
724 lack of mixing loss at coastal stations could partially explain why ammonia oxidation rates can remain similar between
725 coastal and offshore stations (25.8 ± 3.6 vs. 21.3 ± 3.3 nM day^{-1}), yet result in higher accumulated nitrite at a coastal
726 PNM. Modeling efforts that are able to integrate both physical diffusion of nitrite and mixing around the PNM, as
727 well as the influence of environmental fluctuations on microbial rates over longer time scales may be more able to
728 explain observed nitrite concentrations. Additional data from time-integrated approaches such as natural abundance
729 nitrite isotopes would also contribute to estimating nitrite age in the PNM.

730 **4.5 Different time scales inherent to observational patterns**

731 Environmental features may not accurately predict the concentration of the nitrite maximum because of a time lag
732 between environmental conditions measured at a station, the response of the microbial community, and the length of
733 time needed to produce a PNM. Previous work has shown that a seasonal PNM can develop over 6 days in the Gulf
734 of Aqaba (Mackey et al., 2011). In our study, a large range in net production rates was observed (~ 0 - 86.9 nM day^{-1}),
735 leading to the potential for a PNM to develop in less than a day at some locations, or as long as months at other stations.
736 The four southern coastal stations (used to inform the coastal MLR) had the largest nitrite maxima measured in this
737 study (with nitrite concentrations reaching 800-1400 nM). However, it is reasonable to expect that in dynamic coastal
738 waters, upwelling and offshore transport of water would lead to shorter water residence times and less time for nitrite
739 to accumulate in the PNM. Indeed, local surface current data from early April 2016 show the fastest currents occurring
740 along the southern coastline (Fig S8). However, even given these current velocities, nitrite accumulation over the span
741 of days to weeks seems possible. Thus, our nitrite residence time calculations, on the order of days to months, are
742 consistent with the residence time of water in the coastal environment, and other estimates of PNM residence times
743 (Fig. S6). For example, ammonia oxidation measurements from the California Current System suggested an 18-470
744 day residence time for offshore stations, and 40 day residence time for a coastal station (see full table in Santoro et al.
745 2013).

746 **4.6 Spatiotemporal controls on the nitrite maximum**

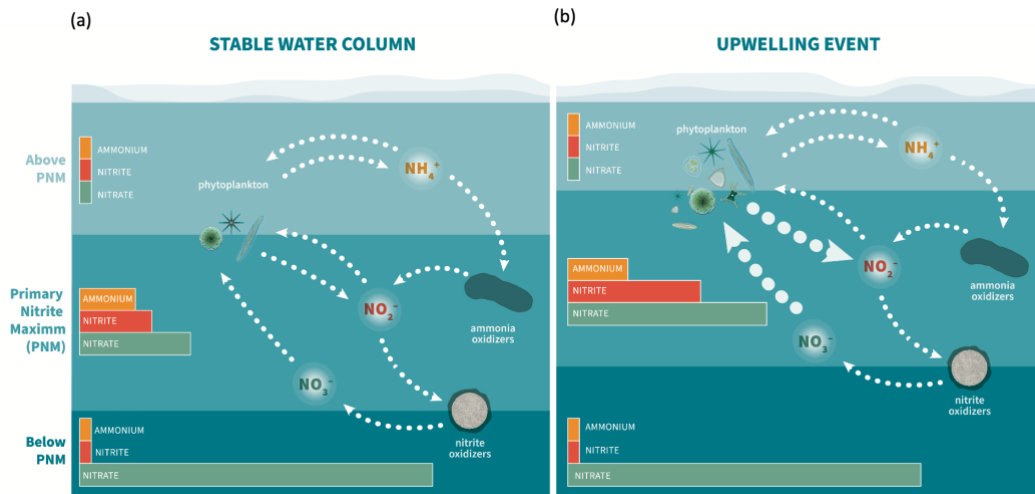
747 Previous work investigating the onset of the PNM has shown that nitrite concentrations are highest at the beginning
748 of seasonal stratification when phytoplankton begin to bloom, suggesting that phytoplankton help provide the
749 necessary conditions for nitrite accumulation (Al-Qutob et al., 2002; Mackey et al., 2011; Meeder et al., 2012; Vaccaro
750 and Ryther, 1960). In Mackey et al. (2011), the onset of stratification initiates a phytoplankton bloom that begins to
751 deplete surface nitrate and releases ammonia via phytoplankton degradation and zooplankton grazing. An
752 accumulation of ammonium forms just below the chlorophyll maximum, which is subsequently followed by an

753 accumulation of nitrite just below the ammonium peak. This continued stratification pattern supports the persistence
754 of the emergent PNM feature, though the size of the nitrite maximum declines over the duration of the stratification
755 period. The correlation between coastal upwelling and higher nitrite accumulation in the ETNP PNM may be
756 controlled by similar mechanisms as the high nitrite accumulation at the onset of seasonal stratification in other regions.
757 Instead of a strongly seasonal onset of stratification, the ETNP stratification persists year-round but is modulated by
758 upwelling along the coast.

759 At coastal stations in 2016, we saw high average concentrations of nitrate ($16 \mu\text{M}$) at the depth of the PNM due to
760 upwelling conditions, while average nitrate concentrations at offshore PNM were lower ($5.9 \mu\text{M}$). The positive
761 correlation of nitrate concentration at the PNM peak with the concentration of the nitrite maximum ($R^2=0.5$, $p=0.01$)
762 suggests that upwelling nitrate is critical for larger nitrite maxima. The correlation found in the MLR analysis between
763 the chlorophyll-nitrate interaction term and the nitrite maxima supports the idea that higher nitrite accumulation
764 requires the presence of higher levels of nitrate within the chlorophyll bloom (Anderson and Roels, 1981). High
765 variation in the correlation of nitrite maxima with chlorophyll, ammonium and nitrate may be due to how recently the
766 chlorophyll bloom was initiated, and whether it has had time to draw down available nitrate. However, these patterns
767 do not identify whether the presence of nitrate drives nitrite production from phytoplankton directly, or indirectly, by
768 stimulating ammonia oxidation.

769 Sequential decomposition of particulate organic nitrogen (PON) produces ammonium, then nitrite, and nitrate over
770 time, and matches the spatial ordering of these species with depth in the water column (Meeder et al. 2012). In a
771 stratified water column, the vertical transport of material may be slow enough to allow for a similar temporal
772 degradation pattern to emerge across the pycnocline. The sequence is initiated by the blooming of phytoplankton,
773 which is restricted to surface depths with adequate light and nitrate. In a coastal upwelling regime, the stratified water
774 column is pushed up towards the surface, and this degradation sequence is modified by enhanced source PON from
775 larger chlorophyll blooms. Larger pools of chlorophyll lead to larger accumulations of ammonium and nitrite. Based
776 on the magnitude of net nitrite production, nitrifiers appear to have a larger potential for net nitrite production at ETNP
777 PNM. The association of nitrification rates with increasing nitrate concentration, which is not a required substrate for
778 nitrification, indicates an indirect connection with phytoplankton activity which is typically dependent on nitrate
779 availability. We suggest that changes in light and nitrate availability initiate a cascade of microbial processes that lead
780 from production to degradation of phytoplankton-based PON, providing a substrate for ammonia oxidation. Enhanced
781 phytoplankton productivity in this scenario should lead to higher rates of nitrite production via ammonia oxidation.

782 **Figure 8. Schematic of nitrite cycling processes and relative DIN pools near the PNM. Panel (a) depicts the**
783 **offshore conditions and panel (b) depicts early upwelling conditions that lead to bloom initiation.**



784

785

786 Figure 8 places the findings in the current study in the context of the sequential physical and biological processes
 787 controlling the PNM feature in the ETNP. The schematic depicts a typical offshore PNM from our study region
 788 observed during stratified, stable water column conditions (Fig. 8a), in contrast to that observed during the onset of
 789 upwelling (Fig. 8b). In each case, the surface ocean is split into 3 layers: above, within, and below the PNM, with the
 790 PNM sitting near the top of the nitracline. Phytoplankton control the availability and supply of DIN above the PNM,
 791 where high light allows for complete drawdown of DIN. In the stable water column (Fig. 8a), phytoplankton are
 792 present in a chlorophyll maximum that is small and stable just above the nitracline consisting of smaller eukaryotes
 793 and cyanobacteria (Legendre-Fixx, 2017). The chlorophyll maximum is small because there is no active upwelling,
 794 and the ambient nitrate at the chlorophyll maximum has been depleted to low concentrations. Phytoplankton fail to
 795 access deeper nitrogen supplies because light levels become inadequate at depth, so the chlorophyll maximum is
 796 balanced at the intersection of the dual requirements for light and upwardly diffused nitrate. A small ammonium peak
 797 develops just below the chlorophyll maximum, and just above the nitrite maximum, deriving from phytoplankton
 798 decomposition processes including grazer activity. The supply of ammonium is adequate to fuel an active nitrifier
 799 community in the PNM layer and below, with average rates of ammonia oxidation and nitrite oxidation near 20 nM
 800 day⁻¹. The net imbalance in the two steps of nitrification is small (few nM day⁻¹), contributing to the small yet stable
 801 accumulation of nitrite at the PNM. Contributions of nitrite from phytoplankton are minimal because they have drawn
 802 down surface nitrate and are subsisting at the edge of a well-established deep nitracline. Although the water column
 803 is stably stratified, the Brunt-Väisälä values are moderate.

804 During an upwelling event (Fig. 8b), an influx of nitrate-rich water into the euphotic zone initiates a phytoplankton
 805 bloom. We see evidence of early upwelling at coastal stations where nitrate concentrations at the chlorophyll
 806 maximum are not completely depleted (average 5.2±3.6 μM), while nitrate at offshore station chlorophyll maxima are
 807 lower (average 0.6±0.4 μM). With phytoplankton growth fueled by new nitrate, the ammonium concentration begins
 808 to increase via degradation and grazing, providing substrate for ammonia oxidizers. Rate measurements show a small

809 increase in average ammonia oxidation rate at coastal stations compared to offshore stations (25.8 ± 3.6 vs. 21.3 ± 3.3
810 nM day^{-1} , respectively). At some coastal stations, a more significant change in the concentration of the nitrite
811 maximum may come from increased phytoplankton nitrite release. Previous work has documented up to $\sim 10\%$ of
812 nitrate uptake can be released as nitrite in laboratory culture experiments, suggesting that locations with high nitrate
813 uptake and active nitrate reduction have the potential for substantial nitrite release from phytoplankton (Collos, 1998).
814 Additionally, the physical upwelling of deep water compresses density layers in the euphotic zone leading to higher
815 Brunt-Väisälä frequencies and lower potential for nitrite diffusion away from the site of production, helping to explain
816 larger nitrite maxima occurring at upwelling sites.

817 With nitrite production in the PNM predominantly linked to ammonia oxidation, this has potential implications for
818 production of nitrous oxide in the upper water column of the ETNP. The ETNP is known to be an important source
819 for atmospheric nitrous oxide (Babbin et al., 2020; Tian et al., 2020), with high accumulations of nitrous oxide in the
820 near surface (Kelly et al., 2021; Monreal et al., 2022). Nitrous oxide production in the near-surface maximum has been
821 linked to a combination of hybrid production from AOA, and bacterial denitrification (Kelly et al., 2021; Monreal et
822 al., 2022; Trimmer et al., 2016). Thus, conditions that favor enhanced ammonia oxidation could also promote enhanced
823 nitrous oxide production and emissions, thereby forming a link between stimulation of high primary productivity and
824 high rates of nitrous oxide production and emission.

825 **5 Conclusions**

826 This study used both high resolution environmental data and direct rate measurements of nitrite cycling processes to
827 explore the factors contributing to PNM formation in ETNP. At our sites, there was a distinct and predictable depth
828 where nitrite accumulated in a peak-shaped PNM feature. Linear regression and multivariate regression analysis with
829 environmental data showed that the top of the nitracline and the top of the oxycline are two major indicators of the
830 depth of the nitrite maximum. Rate measurements also showed distinct peaks in activity that corresponded well with
831 the mean PNM isopycnal for the region. Ammonia oxidation was the dominant nitrite production process at most
832 depths and stations, and nitrifier processes dominated nitrite cycling at and below the PNM. Phytoplankton processes
833 were typically restricted to depths above the PNM, and we report only a handful of high nitrate reduction rates (>20
834 nM day^{-1}) from coastal stations with higher chlorophyll and nitrate concentrations at the PNM. However, even where
835 nitrite production from phytoplankton remains low, we suggest a sequential and competitive dependence of ammonia
836 oxidation rates on phytoplankton processes. The importance of co-occurring environmental conditions and timing of
837 microbial interactions should be considered in further work on what factors determine the formation of large nitrite
838 maxima. For example, both nitrate and light availability may work together to control net nitrite production through
839 sequential processes beginning with upwelling events. Microbial physiological responses remain important in
840 connecting rates of activity to dynamic environmental conditions.

841 **References**

- 842 Al-Qutob, M., Häse, C., Tilzer, M. M., and Lazar, B.: Phytoplankton drives nitrite dynamics in the Gulf of Aqaba,
843 Red Sea, *Mar. Eco. Progress*, 239, 233–239, <https://doi.org/10.3354/meps239233>, 2002.
- 844 Anderson, S. and Roels, O.: Effects of light intensity on nitrate and nitrite uptake and excretion by *Chaetoceros*
845 *curvisetus*, *Mar. Biol.*, 62, 257–261, <https://doi.org/10.1007/BF00397692>, 1981.
- 846 Babbín, A. R., Boles, E. L., Mühle, J., and Weiss, R. F.: On the natural spatio-temporal heterogeneity of South Pacific
847 nitrous oxide, *Nature Comm.*, 11, 1–9, <https://doi.org/10.1038/s41467-020-17509-6>, 2020.
- 848 Beman, J. M., Popp, B. N., and Francis, C. A.: Molecular and biogeochemical evidence for ammonia oxidation by
849 marine Crenarchaeota in the Gulf of California, *The ISME journal*, 2, 429–441,
850 <https://doi.org/10.1038/ismej.2007.118>, 2008.
- 851 Beman, J. M., Popp, B. N., and Alford, S. E.: Quantification of ammonia oxidation rates and ammonia-oxidizing
852 archaea and bacteria at high resolution in the Gulf of California and eastern tropical North Pacific Ocean, *Limnol.*
853 *Oceanogr.*, 57, 711–726, <https://doi.org/10.4319/lo.2012.57.3.0711>, 2012.
- 854 Beman, J. M., Shih, J. L., and Popp, B. N.: Nitrite oxidation in the upper water column and oxygen minimum zone of
855 the eastern tropical North Pacific Ocean, *The ISME journal*, 7, 2192–2205, <https://doi.org/10.1038/ismej.2013.96>,
856 2013.
- 857 Böhlke, J. K., Mroczkowski, S. J., and Coplen, T. B.: Oxygen isotopes in nitrate: new reference materials for ¹⁸O: ¹⁷
858 O: ¹⁶O measurements and observations on nitrate-water equilibration: Reference materials for O-isotopes in nitrate,
859 *Rapid Commun. Mass Spectrom.*, 17, 1835–1846, <https://doi.org/10.1002/rcm.1123>, 2003.
- 860 Brandhorst, W.: Nitrite Accumulation in the North-East Tropical Pacific, *Nature*, 182, 679–679,
861 <https://doi.org/10.1038/182679a0>, 1958.
- 862 Bronk, D. A., Glibert, P. M., and Ward, B. B.: Nitrogen Uptake, Dissolved Organic Nitrogen Release, and New
863 Production, *Science*, 265, 1843–1846, <https://doi.org/10.1126/science.265.5180.1843>, 1994.
- 864 Buchwald, C. and Casciotti, K. L.: Isotopic ratios of nitrite as tracers of the sources and age of oceanic nitrite, *Nature*
865 *Geosci.*, 6, 308–313, <https://doi.org/10.1038/NGEO1745>, 2013.
- 866 Burlacot, A., Richaud, P., Gosset, A., Li-Beisson, Y., and Peltier, G.: Algal photosynthesis converts nitric oxide into
867 nitrous oxide, *Proc Natl Acad Sci USA*, 117, 2704–2709, <https://doi.org/10.1073/pnas.1915276117>, 2020.
- 868 Carlucci, A. F., Hartwig, E. O., and Bowes, P. M.: Biological production of nitrite in seawater, *Mar. Biol.*, 7, 161–
869 166, <https://doi.org/10.1007/BF00354921>, 1970.
- 870 Casciotti, K. L., Böhlke, J. K., McIlvin, M. R., Mroczkowski, S. J., and Hannon, J. E.: Oxygen isotopes in nitrite:
871 analysis, calibration, and equilibration, *Anal. Chem.*, 79, 2427–2436, <https://doi.org/10.1021/ac061598h>, 2007.
- 872 Cline, J. D. and Richards, F. A.: Oxygen deficient conditions and nitrate reduction in the eastern tropical North Pacific
873 Ocean, *Limnol. Oceanogr.*, 17, 885–900, <https://doi.org/10.4319/lo.1972.17.6.0885>, 1972.
- 874 Codispoti, L. A., Friederich, G. E., Murray, J. W., and Sakamoto, C. M.: Chemical variability in the Black Sea:
875 implications of continuous vertical profiles that penetrated the oxic/anoxic interface, *Deep Sea Research Part A.*
876 *Oceanographic Research Papers*, 38, S691–S710, [https://doi.org/10.1016/S0198-0149\(10\)80004-4](https://doi.org/10.1016/S0198-0149(10)80004-4), 1991.
- 877 Collos, Y.: Transient situations in nitrate assimilation by marine diatoms. 2. Changes in nitrate and nitrite following a
878 nitrate perturbation, *Limnol. Oceanogr.*, 27, 528–535, <https://doi.org/10.1.1.597.3625>, 1982a.

879 Collos, Y.: Transient situations in nitrate assimilation by marine diatoms. III. Short-term uncoupling of nitrate uptake
880 and reduction, *J. Exp. Mar. Biol. Ecol.*, 62, 285–295, [https://doi.org/10.1016/0022-0981\(82\)90208-8](https://doi.org/10.1016/0022-0981(82)90208-8), 1982b.

881 Collos, Y.: Nitrate uptake, nitrite release and uptake, and new production estimates, *Mar. Eco. Progress*, 171, 293–
882 301, 1998.

883 Cornec, M., Claustre, H., Mignot, A., Guidi, L., Lacour, L., Poteau, A., D’Ortenzio, F., Gentili, B., and Schmechtig,
884 C.: Deep Chlorophyll Maxima in the Global Ocean: Occurrences, Drivers and Characteristics, *Global Biogeochem*
885 *Cycles*, 35, <https://doi.org/10.1029/2020GB006759>, 2021.

886 Dore, J. E. and Karl, D. M.: Nitrite distributions and dynamics at Station ALOHA, Deep Sea Research Part II: Topical
887 Studies in Oceanography, 43, 385–402, 1996.

888 Dugdale, R. and Goering, J.: Uptake of new and regenerated forms of nitrogen in primary productivity, *Limnol.*
889 *Oceanogr*, 12, 196–206, 1967.

890 Dugdale, R. and Wilkerson, F.: The use of ¹⁵N to measure nitrogen uptake in eutrophic oceans; experimental
891 considerations^{1, 2}, *Limnology and Oceanography*, 31, 673–689, 1986.

892 Eppley, R. W. and Coatsworth, J. L.: Uptake of nitrate and nitrite by *Ditylum Brightwelli* - Kinetics and mechanisms,
893 *Journal of Phycology*, 4, 151–156, <https://doi.org/10.1111/j.1529-8817.1968.tb04689.x>, 1968.

894 Francis, C. A., Roberts, K. J., Beman, J. M., Santoro, A. E., and Oakley, B. B.: Ubiquity and diversity of ammonia-
895 oxidizing archaea in water columns and sediments of the ocean, *Proceedings of the National Academy of Sciences of*
896 *the United States of America*, 102, 14683–14688, <https://doi.org/10.1073/pnas.0506625102>, 2005.

897 Francis, C. A., Beman, J. M., and Kuypers, M. M. M.: New processes and players in the nitrogen cycle: the microbial
898 ecology of anaerobic and archaeal ammonia oxidation, *The ISME Journal*, 1, 19–27,
899 <https://doi.org/10.1038/ismej.2007.8>, 2007.

900 French, D. P., Furnas, M. J., and Smayda, T. J.: Diel changes in nitrite concentration in the chlorophyll maximum in
901 the Gulf of Mexico, *Deep Sea Research Part A. Oceanographic Research Papers*, 30, 707–722,
902 <https://doi.org/10.1073/pnas.0506625102>, 1983.

903 Füssel, J., Lam, P., Lavik, G., Jensen, M. M., Holtappels, M., Günter, M., and Kuypers, M. M.: Nitrite oxidation in
904 the Namibian oxygen minimum zone, *The ISME journal*, 6, 1200–1209, <https://doi.org/10.1038/ismej.2011.178>, 2012.

905 Glibert, P. M., Middelburg, J. J., McClelland, J. W., and Jake Vander Zanden, M.: Stable isotope tracers: Enriching
906 our perspectives and questions on sources, fates, rates, and pathways of major elements in aquatic systems, *Limnol*
907 *Oceanogr*, 64, 950–981, <https://doi.org/10.1002/lno.11087>, 2019.

908 Granger, J. and Sigman, D. M.: Removal of nitrite with sulfamic acid for nitrate N and O isotope analysis with the
909 denitrifier method, *Rapid Communications in Mass Spectrometry*, 23, 3753–3762, <https://doi.org/10.1002/rcm.4307>,
910 2009.

911 Grömping, U.: Relative Importance for Linear Regression in R: The Package relaimpo, *Journal of Statistical Software*,
912 17, 1–27, 2006.

913 Gruber, N.: The marine nitrogen cycle: overview and challenges, *Nitrogen in the marine environment*, 2, 1–50,
914 <https://doi.org/10.1038/nature06592>, 2008.

915 Guerrero, M. A. and Jones, R. D.: Photoinhibition of marine nitrifying bacteria. I. Wavelength-dependent response,
916 *Marine Ecology Progress Series*, 141, 183–192, <https://doi.org/10.3354/meps141183>, 1996.

- 917 Hattori, A. and Wada, E.: Nitrite distribution and its regulating processes in the equatorial Pacific Ocean, in: Deep
918 Sea Research and Oceanographic Abstracts, 557–568, 1971.
- 919 Herbland, A. and Voituriez, B.: Hydrological structure analysis for estimating the primary production in the tropical
920 Atlantic Ocean, *Journal of Marine Research*, 37, 16, 1979.
- 921 Holligan, P. M., Balch, W. M., and Yentsch, C. M.: The significance of subsurface chlorophyll, nitrite and ammonium
922 maxima in relation to nitrogen for phytoplankton growth in stratified waters of the Gulf of Maine, *Journal of Marine*
923 *Research*, 42, 1051–1073, <https://doi.org/10.1357/002224084788520747>, 1984.
- 924 Holmes, R. M., Aminot, A., K rouel, R., Hooker, B. A., and Peterson, B. J.: A simple and precise method for
925 measuring ammonium in marine and freshwater ecosystems, *Canadian Journal of Fisheries and Aquatic Sciences*, 56,
926 1801–1808, <https://doi.org/10.1139/f99-128>, 1999.
- 927 Horak, R. E. A., Qin, W., Bertagnolli, A. D., Nelson, A., Heal, K. R., Han, H., Heller, M., Schauer, A. J., Jeffrey, W.
928 H., Armbrust, E. V., Moffett, J. W., Ingalls, A. E., Stahl, D. A., and Devol, A. H.: Relative impacts of light, temperature,
929 and reactive oxygen on thaumarchaeal ammonia oxidation in the North Pacific Ocean, *Limnology and Oceanography*,
930 63, 741–757, <https://doi.org/10.1002/lno.10665>, 2018.
- 931 Kelly, C. L., Travis, N. M., Baya, P. A., and Casciotti, K. L.: Quantifying Nitrous Oxide Cycling Regimes in the
932 Eastern Tropical North Pacific Ocean With Isotopomer Analysis, *Global Biogeochem Cycles*, 35,
933 <https://doi.org/10.1029/2020GB006637>, 2021.
- 934 Key, R. M., Olsen, A., Van Heuven, S., Lauvset, S. K., Velo, A., Lin, X., Schirnick, C., Kozyr, A., Tanhua, T.,
935 Hoppema, M., Jutterstrom, S., Steinfeldt, R., Jeansson, E., Ishi, M., Perez, F. F., and Suzuki, T.: Global Ocean Data
936 Analysis Project, Version 2 (GLODAPv2), ORNL/CDIAC-162, ND-P093,
937 https://doi.org/10.3334/CDIAC/OTG.NDP093_GLODAPV2, 2015.
- 938 Kiefer, D., Olson, R., and Holm-Hansen, O.: Another look at the nitrite and chlorophyll maxima in the central North
939 Pacific, in: Deep Sea Research and Oceanographic Abstracts, 1199–1208, [https://doi.org/10.1016/0011-7471\(76\)90895-0](https://doi.org/10.1016/0011-7471(76)90895-0), 1976.
- 941 Legendre-Fixx, M.: Drivers of phytoplankton community heterogeneity in the Eastern Tropical North Pacific,
942 Undergraduate Thesis, University of Washington, 2017.
- 943 Lomas, M. W. and Glibert, P. M.: Temperature regulation of nitrate uptake: A novel hypothesis about nitrate uptake
944 and reduction in cool-water diatoms, *Limnol. Oceanogr.*, 44, 556–572, <https://doi.org/10.4319/lo.1999.44.3.0556>,
945 1999.
- 946 Lomas, M. W. and Glibert, P. M.: Comparisons of nitrate uptake, storage, and reduction in marine diatoms and
947 flagellates, *Journal of Phycology*, 36, 903–913, <https://doi.org/10.1046/j.1529-8817.2000.99029.x>, 2000.
- 948 Lomas, M. W. and Lipschultz, F.: Forming the primary nitrite maximum: Nitrifiers or phytoplankton?, *Limnology*
949 *and Oceanography*, 51, 2453–2467, <https://doi.org/10.4319/lo.2006.51.5.2453>, 2006.
- 950 L cker, S., Wagner, M., Maixner, F., Pelletier, E., Koch, H., Vacherie, B., Rattei, T., Damst , J. S. S., Spieck, E., Le
951 Paslier, D., and Daims, H.: A *Nitrospira* metagenome illuminates the physiology and evolution of globally important
952 nitrite-oxidizing bacteria, *Proc. Natl. Acad. Sci. U.S.A.*, 107, 13479–13484, <https://doi.org/10.1073/pnas.1003860107>,
953 2010.
- 954 L cker, S., Nowka, B., Rattei, T., Spieck, E., and Daims, H.: The Genome of *Nitrospina gracilis* Illuminates the
955 Metabolism and Evolution of the Major Marine Nitrite Oxidizer, *Front. Microbio.*, 4,
956 <https://doi.org/10.3389/fmicb.2013.00027>, 2013.

- 957 Mackey, K. R., Bristow, L., Parks, D. R., Altabet, M. A., Post, A. F., and Paytan, A.: The influence of light on nitrogen
958 cycling and the primary nitrite maximum in a seasonally stratified sea, *Prog. Ocean.*, 91, 545–560,
959 <https://doi.org/10.1016/j.pocean.2011.09.001>, 2011.
- 960 Martens-Habbena, W., Berube, P. M., Urakawa, H., de la Torre, J. R., and Stahl, D. A.: Ammonia oxidation kinetics
961 determine niche separation of nitrifying Archaea and Bacteria, *Nature*, 461, 976–979,
962 <https://doi.org/10.1038/nature08465>, 2009.
- 963 McIlvin, M. R. and Altabet, M. A.: Chemical conversion of nitrate and nitrite to nitrous oxide for nitrogen and oxygen
964 isotopic analysis in freshwater and seawater, *Analytical Chemistry*, 77, 5589–5595, <https://doi.org/10.1021/ac050528s>,
965 2005.
- 966 McIlvin, M. R. and Casciotti, K. L.: Technical updates to the bacterial method for nitrate isotopic analyses, *Analytical*
967 *chemistry*, 83, 1850–1856, <https://doi.org/10.1021/ac1028984>, 2011.
- 968 Meeder, E., Mackey, K. R., Paytan, A., Shaked, Y., Iluz, D., Stambler, N., Rivlin, T., Post, A. F., and Lazar, B.: Nitrite
969 dynamics in the open ocean-clues from seasonal and diurnal variations, *Marine Ecology Progress Series*, 453,
970 <https://doi.org/10.3354/meps09525>, 2012.
- 971 Merbt, S. N., Stahl, D. A., Casamayor, E. O., Martí, E., Nicol, G. W., and Prosser, J. I.: Differential photoinhibition
972 of bacterial and archaeal ammonia oxidation, *FEMS microbiology letters*, 327, 41–46, [https://doi.org/10.1111/j.1574-
973 6968.2011.02457.x](https://doi.org/10.1111/j.1574-), 2012.
- 974 Miller, J. and Miller, J.: *Statistics for Analytical Chemistry*, 2nd, Ed., John Willy & Sons, NY, 1988.
- 975 Miller, T. L. based on F. code by A.: *leaps: Regression Subset Selection*, 2020.
- 976 Mincer, T. J., Church, M. J., Taylor, L. T., Preston, C., Karl, D. M., and DeLong, E. F.: Quantitative distribution of
977 presumptive archaeal and bacterial nitrifiers in Monterey Bay and the North Pacific Subtropical Gyre, *Environmental*
978 *Microbiology*, 9, 1162–1175, <https://doi.org/10.1111/j.1462-2920.2007.01239.x>, 2007.
- 979 Monreal, P. J., Kelly, C. L., Travis, N. M., and Casciotti, K. L.: Identifying the Sources and Drivers of Nitrous Oxide
980 Accumulation in the Eddy-Influenced Eastern Tropical North Pacific Oxygen-Deficient Zone, *Global Biogeochemical*
981 *Cycles*, 36, <https://doi.org/10.1029/2022GB007310>, 2022.
- 982 Mulholland, M. R. and Lomas, M. W.: Nitrogen uptake and assimilation, *Nitrogen in the marine environment*, 303–
983 384, 2008.
- 984 Olsen, A., Lange, N., Key, R. M., Tanhua, T., Bittig, H. C., Kozyr, A., Álvarez, M., Azetsu-Scott, K., Becker, S.,
985 Brown, P. J., Carter, B. R., Cotrim da Cunha, L., Feely, R. A., van Heuven, S., Hoppema, M., Ishii, M., Jeansson, E.,
986 Jutterström, S., Landa, C. S., Lauvset, S. K., Michaelis, P., Murata, A., Pérez, F. F., Pfeil, B., Schirnick, C., Steinfeldt,
987 R., Suzuki, T., Tilbrook, B., Velo, A., Wanninkhof, R., and Woosley, R. J.: GLODAPv2.2020 – the second update of
988 GLODAPv2, *Oceanography – Chemical*, <https://doi.org/10.5194/essd-2020-165>, 2020.
- 989 Olson, R. J.: Differential photoinhibition of marine nitrifying bacteria: a possible mechanism for the formation of the
990 primary nitrite maximum, *J. mar. Res.*, 39, 227–238, 1981.
- 991 Peng, X., Fuchsman, C. A., Jayakumar, A., Oleynik, S., Martens-Habbena, W., Devol, A. H., and Ward, B. B.:
992 Ammonia and nitrite oxidation in the Eastern Tropical North Pacific: AMMONIA AND NITRITE OXIDATION IN
993 ETNP, *Global Biogeochemical Cycles*, 29, 2034–2049, <https://doi.org/10.1002/2015GB005278>, 2015.
- 994 Plouviez, M., Shilton, A., Packer, M. A., and Guieysse, B.: Nitrous oxide emissions from microalgae: potential
995 pathways and significance, *J Appl Phycol*, 31, 1–8, <https://doi.org/10.1007/s10811-018-1531-1>, 2019.

- 996 Raimbault, P.: Effect of temperature on nitrite excretion by three marine diatoms during nitrate uptake, *Marine Biology*,
997 92, 149–155, 1986.
- 998 Rajaković, L. V., Marković, D. D., Rajaković-Ognjanović, V. N., and Antanasijević, D. Z.: The approaches for
999 estimation of limit of detection for ICP-MS trace analysis of arsenic, *Talanta*, 102, 79–87, 2012.
- 1000 Sakamoto, C. M., Friederich, G. E., and Codispoti, L. A.: MBARI procedures for automated nutrient analyses using a
1001 modified Alpkem Series 300 Rapid Flow Analyzer, 1990.
- 1002 Santoro, A., Sakamoto, C., Smith, J., Plant, J., Gehman, A., Worden, A., Johnson, K., Francis, C., and Casciotti, K.:
1003 Measurements of nitrite production in and around the primary nitrite maximum in the central California Current,
1004 *Biogeosciences*, 10, 7395–7410, 2013.
- 1005 Santoro, A. E., Casciotti, K. L., and Francis, C. A.: Activity, abundance and diversity of nitrifying archaea and bacteria
1006 in the central California Current, *Environmental Microbiology*, 12, 1989–2006, 2010.
- 1007 Santoro, A. E., Buchwald, C., McIlvin, M. R., and Casciotti, K. L.: Isotopic signature of N₂O produced by marine
1008 ammonia-oxidizing archaea, *Science*, 333, 1282–1285, 2011.
- 1009 Schaefer, S. C. and Hollibaugh, J. T.: Temperature Decouples Ammonium and Nitrite Oxidation in Coastal Waters,
1010 *Environmental Science & Technology*, 51, 3157–3164, <https://doi.org/10.1021/acs.est.6b03483>, 2017.
- 1011 Schleper, C., Jurgens, G., and Jonuscheit, M.: Genomic studies of uncultivated archaea, *Nat Rev Microbiol*, 3, 479–
1012 488, <https://doi.org/10.1038/nrmicro1159>, 2005.
- 1013 Shiozaki, T., Ijichi, M., Isobe, K., Hashihama, F., Nakamura, K., Ehama, M., Hayashizaki, K., Takahashi, K.,
1014 Hamasaki, K., and Furuya, K.: Nitrification and its influence on biogeochemical cycles from the equatorial Pacific to
1015 the Arctic Ocean, *The ISME journal*, 10, 2184, 2016.
- 1016 Sigman, D. M., Casciotti, K. L., Andreani, M., Barford, C., Galanter, M., and Böhlke, J. K.: A Bacterial Method for
1017 the Nitrogen Isotopic Analysis of Nitrate in Seawater and Freshwater, *Anal. Chem.*, 73, 4145–4153,
1018 <https://doi.org/10.1021/ac010088e>, 2001.
- 1019 Smith, J. M., Chavez, F. P., and Francis, C. A.: Ammonium uptake by phytoplankton regulates nitrification in the
1020 sunlit ocean, *PloS one*, 9, e108173, 2014.
- 1021 Strickland, J. D. and Parsons, T. R.: A practical handbook of seawater analysis, 1972.
- 1022 Tian, H., Xu, R., Canadell, J. G., Thompson, R. L., Winiwarter, W., Suntharalingam, P., Davidson, E. A., Ciais, P.,
1023 Jackson, R. B., Janssens-Maenhout, G., Prather, M. J., Regnier, P., Pan, N., Pan, S., Peters, G. P., Shi, H., Tubiello, F.
1024 N., Zaehle, S., Zhou, F., Arneeth, A., Battaglia, G., Berthet, S., Bopp, L., Bouwman, A. F., Buitenhuis, E. T., Chang,
1025 J., Chipperfield, M. P., Dangal, S. R. S., Dlugokencky, E., Elkins, J. W., Eyre, B. D., Fu, B., Hall, B., Ito, A., Joos, F.,
1026 Krummel, P. B., Landolfi, A., Laruelle, G. G., Lauerwald, R., Li, W., Lienert, S., Maavara, T., MacLeod, M., Millet,
1027 D. B., Olin, S., Patra, P. K., Prinn, R. G., Raymond, P. A., Ruiz, D. J., van der Werf, G. R., Vuichard, N., Wang, J.,
1028 Weiss, R. F., Wells, K. C., Wilson, C., Yang, J., and Yao, Y.: A comprehensive quantification of global nitrous oxide
1029 sources and sinks, *Nature*, 586, 248–256, <https://doi.org/10.1038/s41586-020-2780-0>, 2020.
- 1030 Trimmer, M., Chronopoulou, P.-M., Maanoja, S. T., Upstill-Goddard, R. C., Kitidis, V., and Purdy, K. J.: Nitrous
1031 oxide as a function of oxygen and archaeal gene abundance in the North Pacific, *Nat Commun*, 7, 13451,
1032 <https://doi.org/10.1038/ncomms13451>, 2016.
- 1033 Vaccaro, R. F. and Ryther, J. H.: Marine Phytoplankton and the Distribution of Nitrite in the Sea*, *ICES Journal of*
1034 *Marine Science*, 25, 260–271, <https://doi.org/10.1093/icesjms/25.3.260>, 1960.

- 1035 Wada, E. and Hattori, A.: Nitrite metabolism in the euphotic layer of the central North Pacific Ocean, *Limnology and*
1036 *oceanography*, 16, 766–772, 1971.
- 1037 Wada, E. and Hattori, A.: Nitrite distribution and nitrate reduction in deep sea waters, *Deep Sea Research and*
1038 *Oceanographic Abstracts*, 19, 123–132, [https://doi.org/10.1016/0011-7471\(72\)90044-7](https://doi.org/10.1016/0011-7471(72)90044-7), 1972.
- 1039 Wan, X. S., Sheng, H.-X., Dai, M., Zhang, Y., Shi, D., Trull, T. W., Zhu, Y., Lomas, M. W., and Kao, S.-J.: Ambient
1040 nitrate switches the ammonium consumption pathway in the euphotic ocean, *Nat Commun*, 9, 915,
1041 <https://doi.org/10.1038/s41467-018-03363-0>, 2018.
- 1042 Wan, X. S., Sheng, H., Dai, M., Church, M. J., Zou, W., Li, X., Hutchins, D. A., Ward, B. B., and Kao, S.:
1043 Phytoplankton-nitrifier interactions control the geographic distribution of nitrite in the upper ocean, *Global*
1044 *Biogeochem Cycles*, <https://doi.org/10.1029/2021GB007072>, 2021.
- 1045 Ward, B. and Carlucci, A.: Marine ammonia-and nitrite-oxidizing bacteria: serological diversity determined by
1046 immunofluorescence in culture and in the environment, *Applied and environmental microbiology*, 50, 194–201,
1047 <https://doi.org/10.1128/aem.50.2.194-201.1985>, 1985.
- 1048 Ward, B. B.: Temporal variability in nitrification rates and related biogeochemical factors in Monterey Bay, California,
1049 USA, *Mar Ecol Prog Ser*, 292, 97–109, <https://doi.org/10.3354/meps292097>, 2005.
- 1050 Ward, B. B., Olson, R. J., and Perry, M. J.: Microbial nitrification rates in the primary nitrite maximum off southern
1051 California, *Deep Sea Research Part A. Oceanographic Research Papers*, 29, 247–255, [https://doi.org/10.1016/0198-](https://doi.org/10.1016/0198-0149(82)90112-1)
1052 [0149\(82\)90112-1](https://doi.org/10.1016/0198-0149(82)90112-1), 1982.
- 1053 Ward, B. B., Kilpatrick, K. A., Renger, E. H., and Eppley, R. W.: Biological nitrogen cycling in the nitracline,
1054 *Limnology and Oceanography*, 34, 493–513, <https://doi.org/10.4319/lo.1989.34.3.0493>, 1989.
- 1055 Watson, S. W. and Waterbury, J. B.: Characteristics of two marine nitrite oxidizing bacteria, *Nitrospina gracilis* nov.
1056 gen. nov. sp. and *Nitrococcus mobilis* nov. gen. nov. sp., *Archiv für Mikrobiologie*, 77, 203–230, 1971.
- 1057 Xu, M. N., Li, X., Shi, D., Zhang, Y., Dai, M., Huang, T., Glibert, P. M., and Kao, S.: Coupled effect of substrate and
1058 light on assimilation and oxidation of regenerated nitrogen in the euphotic ocean, *Limnol Oceanogr*, 64, 1270–1283,
1059 <https://doi.org/10.1002/lno.11114>, 2019.
- 1060 Yool, A., Martin, A. P., Fernández, C., and Clark, D. R.: The significance of nitrification for oceanic new production,
1061 *Nature*, 447, 999–1002, <https://doi.org/10.1038/nature05885>, 2007.
- 1062 Zafiriou, O. C., Ball, L. A., and Hanley, Q.: Trace nitrite in oxic waters, *Deep Sea Res.*, 39, 1329–1347,
1063 [https://doi.org/10.1016/0198-0149\(92\)90072-2](https://doi.org/10.1016/0198-0149(92)90072-2), 1992.
- 1064 Zakem, E. J., Al-Haj, A., Church, M. J., van Dijken, G. L., Dutkiewicz, S., Foster, S. Q., Fulweiler, R. W., Mills, M.
1065 M., and Follows, M. J.: Ecological control of nitrite in the upper ocean, *Nature Communications*, 9,
1066 <https://doi.org/10.1038/s41467-018-03553-w>, 2018.
- 1067 Zehr, J. P. and Ward, B. B.: Nitrogen Cycling in the Ocean: New Perspectives on Processes and Paradigms, *AEM*, 68,
1068 1015–1024, <https://doi.org/10.1128/AEM.68.3.1015-1024.2002>, 2002.
- 1069
- 1070 **Acknowledgements**
- 1071 The authors acknowledge the captain and crew of the research vessels required to collect this data set:
1072 R/V Ronald Brown, R/V Sikuliaq, R/V Sally Ride and the R/V Falkor. We also acknowledge shipboard

1073 support from Marguerite Blum and Matt Forbes. This research was supported by U.S.-NSF grant
1074 OCE1657868 to K. L. Casciotti.

1075

1076 **Author Contributions**

1077 Major data collection efforts, data processing/analysis and writing were conducted by N. Travis.
1078 Significant support during data collection was provided by C. Kelly and M. Mulholland, with additional
1079 contributions during manuscript editing. K. Casciotti was instrumental in initial project design, laboratory
1080 analysis, data investigations and manuscript writing.